A new method to quantify the real supply of mafic components to a hybrid andesite

Article *in* Mineralogy and Petrology · September 2013

DOI: 10.1007/s00410-012-0805-x

CITATIONS
40

READS
358

6 authors, including:

Marie Edmonds
University of Cambridge
192 PUBLICATIONS **6,802** CITATIONS
SEE PROFILE

Melissa Plail
University of the Witwatersrand
15 PUBLICATIONS **313** CITATIONS
SEE PROFILE

Jenni Barclay
University of Bristol
150 PUBLICATIONS **6,000** CITATIONS
SEE PROFILE

Contrib Mineral Petrol
DOI 10.1007/s00410-012-0805-x

ORIGINAL PAPER

A new method to quantify the real supply of mafic components to a hybrid andesite

M. C. S. Humphreys · M. Edmonds · M. Plail · J. Barclay · D. Parkes · T. Christopher

Received: 27 February 2012 / Accepted: 27 August 2012

Abstract The eruption of Soufrière Hills Volcano, Montserrat, has been ongoing since 1995. The volcano is erupting a crystal-rich hornblende-plagioclase andesite with ubiquitous mafic inclusions, indicating mixing with mafic magma. This mafic magma is thought to be the driving force of the eruption, supplying heat and volatiles to the andesite resident in the magma chamber. As well as producing macroscopic mafic inclusions, the magma mixing process involves incorporation of phenocrysts from the andesite into the mafic magma. These inherited phenocrysts show clear disequilibrium textures (e.g. sieved plagioclase rims and thermal breakdown rims on hornblende). Approximately 25 % of all phenocrysts in the andesite show these textures, indicating very extensive mass transfer between the two magma types. Fragments of mafic inclusions down to sub-mm scale are found in the andesite, together with mafic crystal clusters, which are commonly found adhered to the rims of phenocrysts with disequilibrium features. Mineral chemistry also points to the transfer of microlites or microphenocrysts, initially formed in the mafic inclusions, into the andesite. This combined evidence suggests that some of the mafic inclusions disaggregate during mingling and/or ascent, possibly due to shearing, and raises the question: What proportion of the andesite 'groundmass' actually originated in the mafic inclusions, and thus, what is the true amount of mafic magma in the magmatic system? We present a new method for quantifying the relative proportions of groundmass plagioclase derived from mafic and andesitic magma, based on analysis of back-scattered electron images of the groundmass. Preliminary results indicate that approximately 16 % of all groundmass plagioclase belongs genetically to the mafic inclusions. Together with the crystal clusters, disequilibrium phenocryst textures and mm-scale inclusions, there is a 'cryptic' mafic component in the andesite of approximately 6 % by volume. This is significant compared with the proportion of macroscopic mafic inclusions (typically ~ 1–5 %). The new method has the potential to allow tracking of the mafic fraction through time and thus to yield further insights into magma hybridisation processes.

Keywords Magma mixing · Hybridisation · Mafic inclusion · Disaggregation · Microlites · Soufrière Hills Volcano

Communicated by J. Blundy.

Electronic supplementary material The online version of this article (doi:10.1007/s00410-012-0805-x) contains supplementary material, which is available to authorized users.

M. C. S. Humphreys (✉)
Department of Earth Sciences, University of Oxford, South Parks Road, Oxford OX1 3AN, UK
e-mail: madeleine.humphreys@earth.ox.ac.uk

M. Edmonds · D. Parkes
Department of Earth Sciences, University of Cambridge, Downing Street, Cambridge CB2 3EQ, UK

M. Plail · J. Barclay
School of Environmental Sciences, University of East Anglia, Norwich Research Park, Norwich NR4 7TJ, UK

T. Christopher
Montserrat Volcano Observatory, Flemings, Montserrat, West Indies

Introduction

At many arc volcanoes, recharge of the volcanic system by a different magma is cited as the trigger for eruptions. The

Published online: 18 September 2012

recharge magma can be of a similar composition, or more silicic than the host magma, but is most commonly more mafic (Sparks et al. 1977; Wiebe 1987; Eichelberger et al. 2000; Humphreys et al. 2006). Mafic recharge involves strong temperature and viscosity contrasts between the host and intruding magma and results in mingling, typically manifest as mafic inclusions (enclaves), or banded magmas. The mafic inclusions have a characteristic diktytaxitic texture resulting from crystallisation at high undercooling (Bacon 1986). Closer mixing (hybridisation) is most likely to occur in magmas of similar viscosity and temperature, or where the proportions of the two magmas are similar (Sparks and Marshall 1986).

The effects of interaction between magmas of two different compositions are also seen in disequilibrium phenocryst textures, such as partial dissolution (e.g. sieve texture in plagioclase) or reaction and overgrowth rims (e.g. clinopyroxene on quartz), produced when crystals from one magma are in contact with the melt from another (e.g. Eichelberger 1978). Such crystal-scale disequilibrium textures are commonly observed at subduction zone settings. Evidence for mixing or hybridisation has now been recognised at all scales in several magmatic systems, such as Lassen Volcanic Center, California (Tepley et al. 1999; Clynne 1999) and Tatara-San Pedro, Chile (Feeley and Dungan 1996). Disaggregation of mafic inclusions after mingling causes the dispersal of disequilibrium-textured crystals back into the andesite, together with small fragments and crystal clusters of mafic inclusions. These processes can also be detected at Soufrière Hills Volcano, Montserrat (Humphreys et al. 2009a). There must therefore be substantially more mafic magma in the volcanic system than would be identified by the macroscopic mafic inclusions themselves. An ability to quantify this dispersed, cryptic component would improve our understanding of temporal trends in mafic magma supply, the dynamics of the volcanic system, and in more general terms, the genesis of andesite magmas. Quantifying the supply and incorporation of mafic magma into the hybrid host magma is also important for understanding the significance of other monitoring data sets such as gas emissions (Edmonds et al. 2010) and ground deformation (Elsworth et al. 2008).

Previous attempts to quantify the extent of mixing typically involve either basic mass balance calculations (e.g. Clynne 1999; Druitt et al. 2012) or identification of a particular type of phenocryst texture (e.g. Kent et al. 2010; Druitt et al. 2012). For example, Druitt et al. (2012) identified a 'Type 1' plagioclase (with calcic core and sodic overgrowth) in the hybrid Santorini rhyodacite as originating in a dacitic magma. The proportion of Type 1 crystals in the resulting hybrid then allowed the proportion of dacite in the mixed magma to be estimated as 7–35 %. However, these methods ignore the other cryptic components of mixing (the fine-grained bulk of the mafic inclusions themselves, and any residual liquid) and assume that the compositions of the end-member magmas are themselves unhybridised and do not change with time, so that any bulk rock compositional variations must be related to hybridisation.

In this study, we present a new method to quantify the amount of dispersed, mafic inclusion material in the Soufrière Hills andesite magma, by processing and binning anorthite contents of plagioclase determined from Scanning Electron Microscope (SEM) images, which are capable of dealing with large sample areas. We show that the dispersed component is substantial and increases our estimates of mafic magma abundance at Soufrière Hills Volcano by several per cent, which is significant in comparison with the abundance of macroscopic inclusions ($\sim$5 % in Phase III of the current eruption; Barclay et al. 2010).

Background

Geological background

Soufrière Hills Volcano (SHV) lies at the southern end of the island of Montserrat, in the Lesser Antilles approximately 35 miles southwest of Antigua. Volcanism is a result of westward subduction of the Atlantic plate underneath the Caribbean plate at around 20–40 mm/year (Macdonald et al. 2000). Harford et al. (2002) identified four separate volcanic centres with ages up to $\sim$2.6 Ma, which show that volcanism has migrated southward over time. The currently active complex, the Soufrière Hills, occupies the southern part of the island and comprises a central dome complex and surrounding fan of pyroclastic debris (Harford et al. 2002). The active dome sits within an existing crater (English's Crater) from past eruptive activity, and the oldest rocks from Soufrière Hills are at least $\sim$170 ka old (Harford et al. 2002). Most of the volcanic products are andesitic with a minor mixed mafic component, with the exception of South Soufrière Hills (SSH) lava, which is basaltic to basaltic andesite in composition. Geochemical studies have shown that the mafic inclusions present in the andesite are not derived from the SSH mafic lavas, but that the SHV andesites can be produced by fractional crystallisation of the SSH magma (Zellmer et al. 2003).

Soufrière Hills Volcano has been erupting again since July 1995, following a period of elevated seismicity that started in 1992. The eruption started with a series of phreatic explosions that were followed by the emplacement of andesitic lava at a summit lava dome (Sparks et al. 2000). The eruption has comprised episodes of lava dome

extrusion sometimes accompanied by significant explosive activity, and pauses, where active extrusion at the dome ceased. Degradation and gravitational destabilisation of the lava dome occurs during both active extrusion and pauses, and several significant dome collapses have also occurred. Extrusion rates are typically on the order of ~2–3 m^3/s but have reached 20 m^3/s (between January and March 2007; Ryan et al. 2010).

Andesite petrology

The SHV lava is a highly porphyritic, hornblende-plagioclase andesite. Typically, plagioclase accounts for ~70 % of all phenocrysts, with ~20 % hornblende, 5 % orthopyroxene, 3 % oxides and rare quartz. Plagioclase textures are highly variable but can typically be classified as sieved (Fig. 1b), patchy-cored or oscillatory zoned (e.g. Murphy et al. 2000). Hornblende phenocrysts may show broad oscillatory zonation but this can be hard to identify optically. Hornblende is commonly out of equilibrium and this is reflected in a number of breakdown textures, including thermal decomposition (Fig. 1c), decompression breakdown rims and opacitisation (e.g. Devine et al. 1998; Murphy et al. 2000; Devine et al. 2003; Rutherford and Devine 2003). Fe–Ti oxide phenocrysts are commonly rounded or with fritted margins but microlites are euhedral. Quartz is either rounded and deeply embayed or surrounded by a rim of small clinopyroxene crystals. Orthopyroxene phenocrysts may be euhedral or slightly rounded or show a Mg-rich overgrowth rim or jacket of clinopyroxene crystals (Fig. 1d). Rare clusters of sector-zoned clinopyroxene microphenocrysts are also found but their origin is unclear and could be related to incorporation of cumulate or crustal xenoliths (Kiddle et al. 2010). The groundmass contains microlites of plagioclase, orthopyroxene, clinopyroxene and oxides and is commonly vesicular. Accessory minerals include apatite and very rare zircon. In some samples, spherulites of intergrown feldspar and quartz are found, typically nucleating on small feldspar microlites. In dome rocks, the groundmass glass commonly undergoes phase separation into patches that are rich in Fe and K, and patches that are rich in Ca and Na. This is similar to that observed in the groundmass at Mount St Helens, which was interpreted to reflect post-extrusive textural modification during prolonged storage in the dome (Cashman 1992). Cristobalite is commonly found filling vesicles in dome rocks and is thought to result from vapour phase deposition due to gas flow through permeable rocks (Baxter et al. 1999).

Mafic inclusion petrology

A key feature of the erupted products is the presence of ubiquitous mafic inclusions (Fig. 1a), which are also commonly observed in older eruptive products on Montserrat and at many other volcanoes worldwide. These mafic inclusions may be a manifestation of the driving force for eruption (Sparks et al. 2000), as observed elsewhere. Mafic inclusions have been reported to occur in SHV andesites as old as 24 ka (Wadge and Isaacs 1988), which indicates that intrusion of mafic magma into the system is a fundamental and continuing feature of volcanism on Montserrat. Murphy et al. (1998) describe the inclusions as dominantly ellipsoidal, with sharply defined, smooth or crenulated, sometimes chilled margins to the host andesite, suggesting that they were incorporated into the host magma while still fluid. However, a proportion of the inclusions have sharp, angular margins, suggesting brittle break-up of larger inclusions or rafts of the mafic material (Plail et al. 2012).

The mafic inclusions are typically fine-grained, 1–80 cm in diameter and with a randomly oriented, inter-locking crystal framework (Fig. 1e) that suggests rapid quench crystallisation (Bacon 1986; Murphy et al. 1998). Most are vesicular, with porosities ranging from 11 to 25 vol%, and some inclusions have a glassy rim (Plail et al. 2012). Most inclusions contain a minor component of coarse crystals, giving them a porphyritic appearance. However, the compositions and textures of these coarse crystals (of plagioclase, hornblende or orthopyroxene) indicate that they are not phenocrysts that grew in equilibrium with the mafic melt. Instead, they represent phenocrysts from the host andesite that are incorporated into the mafic inclusions during the mingling or mixing process while the mafic magma was still fluid, possibly as a result of shearing at the boundary between two magmas (Kouchi and Sunagawa 1985). Hence, the large plagioclase typically have a sieve-textured zone overgrown by a new, Ca-rich rim; orthopyroxenes and rare quartz are typically overgrown by a jacket of fine-grained clinopyroxene; and hornblendes show a thermal breakdown texture (Murphy et al. 1998; Devine et al. 2003; Humphreys et al. 2009a; Plechov et al. 2008). These thermal breakdown rims are distinct from decompression breakdown rims (which can also be observed in hornblendes in the andesite) because they are markedly more clinopyroxene-rich; individual cpx are also aligned parallel to the c-axis of the hornblende, whereas in decompression breakdown rims, there is no preferential alignment (Devine et al. 2003; Browne et al. 2006; Humphreys et al. 2009a, b; Plechov et al. 2008). They can also contain abundant apatite. However, when the rims are fine-grained and poorly developed, the two textures can be very difficult to distinguish. It is notable, however, that plagioclase inclusions in either thermally decomposing hornblendes or in orthopyroxenes with cpx overgrowths commonly themselves show incipient sieve texture; this sieving of included plagioclases may therefore be used as

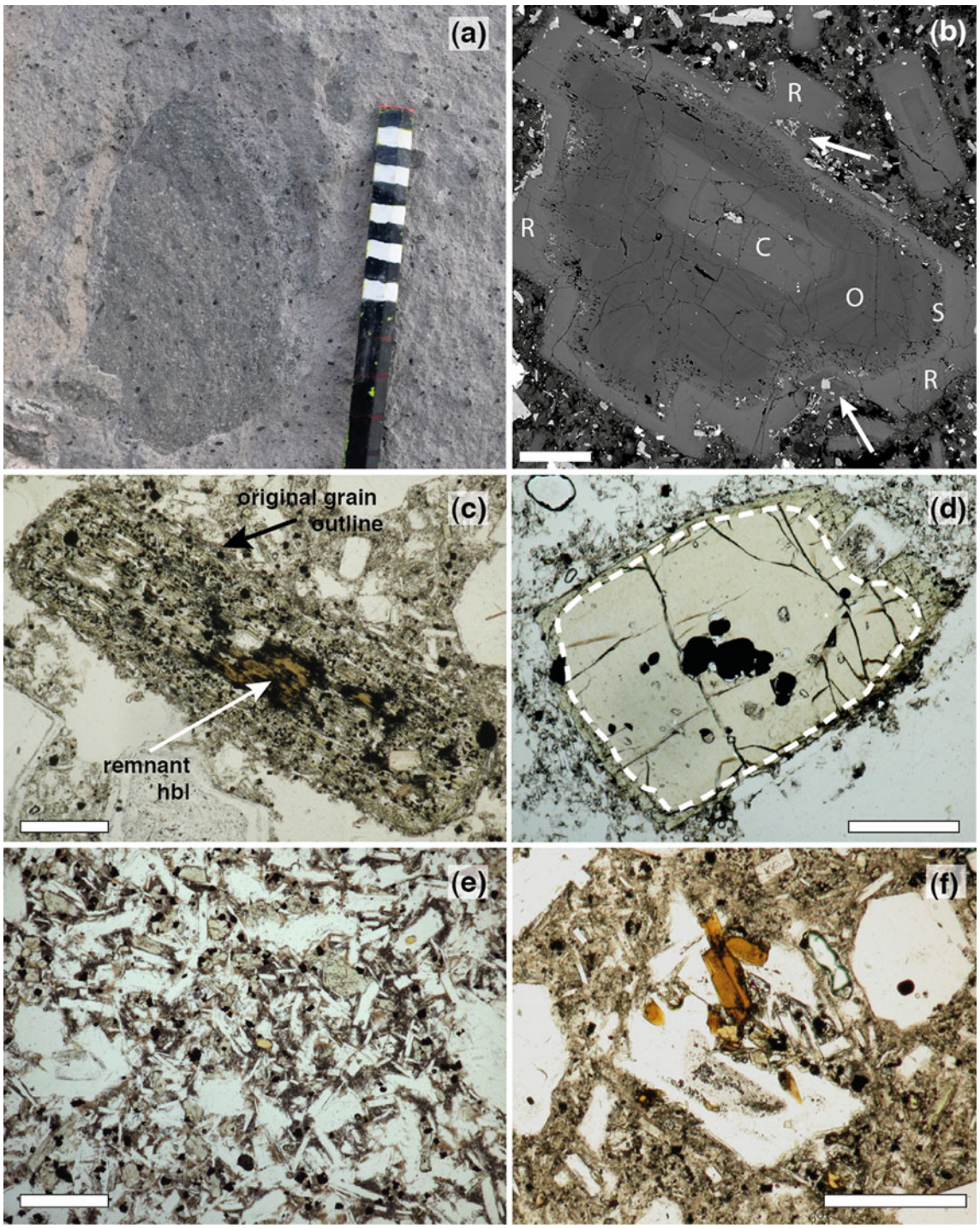

Fig. 1 **a** Typical mafic inclusion from Phase III of the Soufrière Hills Volcano eruption. The *scale bar* shows 1 cm gradations. **b** Back-scattered SEM image showing a plagioclase phenocryst from the andesite with calcic core (*C*), oscillatory zoned region (*O*), sieved ring (*S*) and calcic overgrowth rim (*R*). *Arrows* point to adhered glassy material with compositions and textures similar to those of the mafic inclusions. *Scale bar* 200 μm. **c** Photomicrograph of thermally decomposed amphibole in the andesite. The remnant original core has also undergone opacitisation during shallow dome storage. The thermal breakdown rim has abundant cpx aligned with the c-axis of the original amphibole grain. *Scale bar* 400 μm. **d** Photomicrograph of thermal reaction rim on orthopyroxene phenocryst in the andesite. The orthopyroxene core is overgrown by a rim of new cpx crystals marked by *dashed line*. *Scale bar* 400 μm. **e** Photomicrograph showing typical groundmass texture of a mafic inclusion, with plagioclase, clinopyroxene, orthopyroxene, Fe–Ti oxides, matrix glass and some patches of devitrified glass. *Scale bar* 400 μm. **f** Photomicrograph of a crystal cluster in the andesite, interpreted as part of a disaggregated mafic inclusion. Identifiable characteristics include *yellowish* pargasitic amphibole, sieve-textured plagioclase microphenocryst with amphibole in the overgrowth rim, and diktytaxitic texture which is clearly distinct from that of the andesite groundmass. *Scale bar* 400 μm

an additional constraint to understanding the origin of large mafic crystals.

Samples studied

We studied nine samples of the andesite dating from September 2002 (MVO1234, Phase III) to July 2008 (MVO1532, Phase V), and one representative mafic inclusion that erupted in the summer 2006 (MVO1448), using different methods (Table 1). Five of the andesite samples were taken from one individual flow and were analysed to get an idea of the likely heterogeneity of the textures on a larger scale. Point counting of phenocryst textures and crystal clusters was performed on all nine andesite samples. We also analysed the textures of large crystals in the mafic inclusion sample. Image analysis of plagioclase greyscale distributions (see later) was done on one sample of the andesite (MVO1445) and the mafic inclusion sample (MVO1448).

Quantifying the true abundance of mafic magma

The proportion of macroscopic mafic inclusions

Quantifying the volumetric importance of mafic magma in any volcanic system is crucial for understanding the significance of other monitoring data sets such as gas emissions (Edmonds et al. 2010) and ground deformation (Elsworth et al. 2008), as well as for understanding the significance of changes in eruptive behaviour such as extrusion rate, which might be influenced by changes in magma viscosity and magma chamber pressure (Melnik and Sparks 1999). Existing estimates of the volumetric fraction of mafic magma in Soufrière Hills Volcano erupted products are derived from the abundance of macroscopic mafic inclusions, approximately 1–2 % on the basis of qualitative examination of andesite outcrops from Phase I (Murphy et al. 1998). Barclay et al. (2010) employed a similar, but more quantitative, field-scale 'point-counting' method to study several large blocks of lava emplaced during Phase III of the eruption and estimated the abundance of mafic inclusions as 5–7 %. It was suggested that this might represent a significant and meaningful increase in the proportion of mafic magma in the system, perhaps indicating that a mixing episode had occurred during the course of the eruption (Barclay et al. 2010). Komorowski et al. (2010) also reported a very high proportion of mafic material from sieveing of tephra from the 29 July 2008 explosion fallout: as many as 12.3 % of 301 clasts in the 32–64 mm size fraction were (or contained significant) mafic material. These tephra samples may have been subject to aeolian winnowing prior to examination, however, so this result should be treated with caution.

These field-based estimates of macroscopic mafic magma abundance at Soufrière Hills Volcano are consistent with those at other arc volcanoes and intrusive suites. For example, the proportion of mafic inclusions is estimated at 4.1 % for the Cape Akrotiri rhyolites, Santorini, Greece (Mortazavi and Sparks 2004); 2–10 % for Southwest Trident volcano, Alaska (Coombs et al. 2002); approximately 1 % for Unzen Volcano, Japan (Browne et al. 2006); 2.7–16.4 % for Chaos Crags, Lassen Volcanic Center (Stout et al. 2007); and 3–19 % for the Mt Helen dome, Lassen Volcanic Center, California (Feeley et al. 2008). In the plutonic environment, mafic inclusion abundances are reported as ~5 % for the Cobo Granite, Guernsey, UK (D'Lemos 1996) and 2–5 % for the Adamello Massif, Italy (Blundy and Sparks 1992). There may be evidence of local and temporal variations in mafic magma abundance within the host magma. For example, D'Lemos (1996) reports significant variations in mafic magma distribution within the Cobo Granite, citing in particular that the larger inclusions are surrounded by many smaller ones. This is echoed by McLeod et al. (2011) who describe partially digested, lenticular inclusions with wispy margins close to larger dioritic bodies in the Ross of Mull Granite, Isle of Mull, Scotland, with a local abundance of up to 20 %. The abundance of mafic inclusions increases towards the margins of intrusive sheets in the Adamello pluton, by up to a factor of 10 (2 inclusions per m^2, up to 20 per m^2; Blundy and Sparks 1992). An increase in mafic inclusion abundance has been observed in the later units erupted at Chaos Crags, Lassen Volcanic Center, California (Heiken and Eichelberger 1980; Stout et al. 2007). Many of these observations are from intrusive centres, but this is probably because of the ease of access and exposure at these sites; there is no reason to believe that the same processes are not also occurring beneath currently active volcanic centres.

Sparks and Marshall (1986) considered the physics and rheological implications of mixing between lower density, silicic magma and higher density, more mafic magma. They identified three possible mechanical regimes for the mingled products: (1) the mafic magma remains less viscous than the silicic after mixing; (2) the mafic magma becomes more viscous than the silicic magma after mixing; and (3) the mafic magma effectively solidifies. Regime (1) could result in complete mixing or hybridisation, (2) could result in a variety of fabrics including flow banding, and (3) could result in quenched mafic inclusions. Taking into account considerations of thermal equilibration, hybridisation is more likely when the proportion of mafic magma in the system is relatively large or when the viscosities of the two liquids are similar, while the formation of solid inclusions is favoured when the volumetric proportion of mafic magma is small and/or if the viscosity contrast is

Table 1 Relative proportion of disequilibrium phenocryst textures as identified in samples of the andesite

Sample	Sample type	Date erupted	Sieved plag	Total plag	% sieved	Thermally decomposed hbl	Total hbl (incl. not sure)	% thermally decomposed	Cpx-rimmed opx	Total opx	% cpx-rimmed	% crystal clusters	Estimated groundmass vesicularity	Normalised % crystal clusters
MVO1532a	Andesite, pumice	28th July 2008	40	108	37	5	17	29	2	8	25	0.05	59	0.12
MVO1532c	Andesite, dome rock	28th July 2008	65	245	27	9	43	21	1	20	5	2.35	21	2.97
MVO1445	Andesite, dome rock	20th May 2006	72	323	22	12	29	41	1	11	9	0.31	27	0.42
MVO1234-1	Andesite, dome rock	21st-29th September 2002	88	250	35	6	36	17	9	31	29	0.28	40	0.47
MVO1234-2	Andesite, dome rock	21st-29th September 2002	58	247	23	5	24	21	2	14	14	1.4	39	2.30
MVO1234-3	Andesite, dome rock	21st-29th September 2002	65	264	25	5	28	18	4	21	19	0.24	16	0.29
MVO1234-4	Andesite, dome rock	21st-29th September 2002	72	285	25	6	34	18	2	20	10	–	25	–
MVO1234-5	Andesite, dome rock	21st-29th September 2002	62	226	27	3	35	9	4	15	27	0.18	33	0.27
MVO1236Loc33	Andesite, dome rock	12th July 2003	81	387	21	5	22	23	0	21	0	0.44	24	0.58
MVO1448	Mafic inclusion	30th June 2006	70	93	75	9	16	56	10	13	77			
Average (andesite)					27.0			21.8			15.3	0.7	31.6	0.9

large (Sparks and Marshall 1986). The amount of mafic magma should be relatively straightforward to quantify in regime (3) but would be much harder to quantify if any degree of hybridisation has occurred, or if any of the inclusions had broken down into smaller fragments.

Estimating the microscopic proportion of mafic-derived material in the host magma

Following the previous discussion, an important question for attempting to quantify the true involvement of mafic magma is the extent to which microscopic fragments of mafic inclusions may have been incorporated into the host magma during hybridisation or mingling. Several studies have identified mafic-derived material on a range of scales down to microscopic fragments or individual crystals (e.g. Crater Lake, Oregon, Nakada et al. 1994; Chaos Crags, Lassen Volcanic Center, Tepley et al. 1999; Lassen Peak, California, Clynne 1999; Volcan Tatara San Pedro, Chile, Feeley and Dungan 1996; Mont Pelée, Martinique, Martel et al. 2006). Such identifications are typically made on the basis of careful petrography and geochemical analysis. The implication of these observations is that a proportion of the larger mafic inclusions partially disaggregated at some time after mingling took place; the true proportion of mafic magma in the system is therefore much greater than that observed in the abundance of macroscopic mafic inclusions. Similar observations have been made at Soufrière Hills Volcano (Humphreys et al. 2009a), where, as well as the presence of microscopic crystal clusters and disequilibrium phenocrysts (Fig. 1f), there is a strong compositional overlap between the plagioclase, orthopyroxene and clinopyroxene microlites that are found in the andesite, and the compositions of those minerals in mafic inclusions. Humphreys et al. (2009a) interpreted this as evidence for even more significant disaggregation of inclusions, probably while still plastic, and dispersal of individual microlites into the groundmass of the host andesite. Given this array of evidence for 'cryptic' dispersal of mafic-derived components into the host magma, we require additional methods in order to quantify the true importance of mafic magma in the system. The use of simple mass balance calculations, following Clynne (1999) and using end-member bulk rock compositions of 51 wt% SiO_2 for the mafic magma and 58.5–61 wt% SiO_2 for the andesite (Murphy et al. 2000), suggests approximately 25 % dispersed mafic material in the andesite. However, this assumes that all the chemical variation can be ascribed to hybridisation and that the mafic end-member is not already a hybrid magma.

Abundance of small crystal clusters

As an alternative, we used two simple point-counting methods to quantify the proportion of mafic-derived material. The first method involved image analysis to quantify the abundance of small crystal clusters in the andesite (Fig. 1f). The crystal clusters were identified by their texture, which is similar to that observed in the mafic inclusions; the distinctive yellow, aluminium-rich amphibole that is commonly found in the mafic inclusions (Murphy et al. 2000) may also be present. The estimate of the volume fraction of crystal clusters is almost certainly a minimum since we relied (in part) on the presence of amphibole, which is present only in a subset of mafic inclusions (Murphy et al. 2000; Plail et al. 2012). The margins of the crystal clusters were outlined on high-resolution scans of each thin section and the area quantified using ImageJ (Rasband 1997–2011); the results are reported in Table 1. The area occupied by these crystal clusters varied from 0.05 to 2.35 % of the total area of a thin section; the average (measured across nine samples) was 0.7 %. When we correct for the vesicularity of each sample (typically 20–40 %), these values increase to 0.1–3.0 % (Table 1). The samples with the highest values clearly show mm-sized mafic inclusions in addition to clusters of 1–10 grains.

Relative abundance of disequilibrium textures

The second method we used to get an indication of the importance of mixing was to quantify the relative abundance of phenocryst disequilibrium textures in the andesite, where the textures can be identified explicitly as having resulted from contact with hotter, more mafic magma. In the Soufrière Hills magma, sieved plagioclase, thermally decomposed amphiboles, and orthopyroxene and quartz with clinopyroxene overgrowths are generally agreed to represent such effects (e.g. Murphy et al. 2000; Devine et al. 1998; Humphreys et al. 2009a). We therefore quantified the relative proportions of (1) plagioclase phenocrysts whose outermost major zone showed sieve texture followed by a clear rim, (2) amphiboles that had undergone thermal breakdown, and (3) orthopyroxenes with clinopyroxene reaction rims, not including those with a simple Mg-rich overgrowth rim. We did not include quartz because it is sufficiently uncommon (typically only 1 or 2 grains per thin section) that the results would not be significant or reliable. The thermal breakdown rim for amphibole is relatively simple to recognise in certain crystallographic orientations by its cpx-rich nature with aligned crystals, but can be hard to differentiate from decompression breakdown rims, particularly when relatively fine-grained. We therefore took a cautious approach, counting only those crystals with fairly clear thermal breakdown textures. The results are reported in Table 1. Sieved plagioclase accounted for 21–37 % of all plagioclase phenocrysts (mean $\sim$27 %, $n = 2335$). Thermally

decomposed amphiboles accounted for 9–41 % of all amphibole phenocrysts (mean ~ 22 %, $n = 268$), and orthopyroxene crystals with rims of clinopyroxene were 0–29 % of all orthopyroxenes (mean ~ 15 %, $n = 161$). These results are similar to the basic mass balance calculation (see earlier) and suggest that approximately one quarter of all phenocrysts have at some point interacted with hotter, more mafic magma, for a sufficient length of time to allow the crystals to undergo reaction and re-equilibration with their new surroundings. For comparison, in the mafic inclusion sample MVO1448, approximately 75 % of all large plagioclase crystals were sieved, 77 % of all orthopyroxenes had cpx overgrowth rims, and 56 % of the large amphiboles had unambiguous thermal breakdown rims (Table 1). This supports the argument that it is incorporation of crystals into this new disequilibrium environment that results in these characteristic textures.

The anorthite distribution of groundmass plagioclase

There is a strong compositional correspondence between plagioclase, orthopyroxene and clinopyroxene in the andesite groundmass, and the compositions of those minerals in the mafic inclusions (Humphreys et al. 2009a). In particular, for plagioclase, both the microlites and mafic compositions are typically very An-rich (up to An_{95}) and richer in Fe and Mg than the phenocrysts (see Fig. 2 in Humphreys et al. 2009a). This compositional overlap also occurs in the andesites of Mt Pelée, Martinique (Martel et al. 2006), and has been interpreted as an indication that small, mafic-derived, anomalously An-rich crystals were transferred into the host andesite during disaggregation of the mafic inclusions (Clynne 1999; Martel et al. 2006; Humphreys et al. 2009a), although this argument was rejected by Couch et al. (2003) on the basis of a lack of groundmass amphibole, which is observed in some of the mafic inclusions (Plail et al. 2012).

To try to quantify the relative abundance of these mafic-derived microlites, we analysed the anorthite distribution (or 'X_{An} distribution') of small plagioclase crystals in the groundmass of the Soufrière Hills andesite. We developed a new method using image analysis to assess the volumetric proportions of different plagioclase compositions in the groundmass. We used this method to analyse the X_{An} distributions of small plagioclase crystals in the andesite groundmass, as well as populations of plagioclase in a mafic inclusion for comparison. In order to test objectively the accuracy of the fitting procedures, we also produced some 'synthetic' crystals with a bright grey core and darker grey rim of known intensities using a drawing software package. For these synthetic crystals, we calibrated the greyscale intensities of the core and rim to give the desired range of X_{An} ratios, added Gaussian noise of a fixed standard deviation and then analysed the 'X_{An}' distributions in the same way as the natural samples.

Methods

Analytical methods

We used a JEOL-JSM-840 scanning electron microscope at the University of Oxford to collect back-scattered electron images of a sample of the andesite and a mafic inclusion (samples MVO1445 and MVO1448, see Table 1). The instrumental setup used a 20-kV accelerating voltage and 15 mm working distance. Back-scattered electron (BSE) contrast and brightness conditions were optimised in each image. Images were collected using 'Kalman' style acquisition over 15–20 frames.

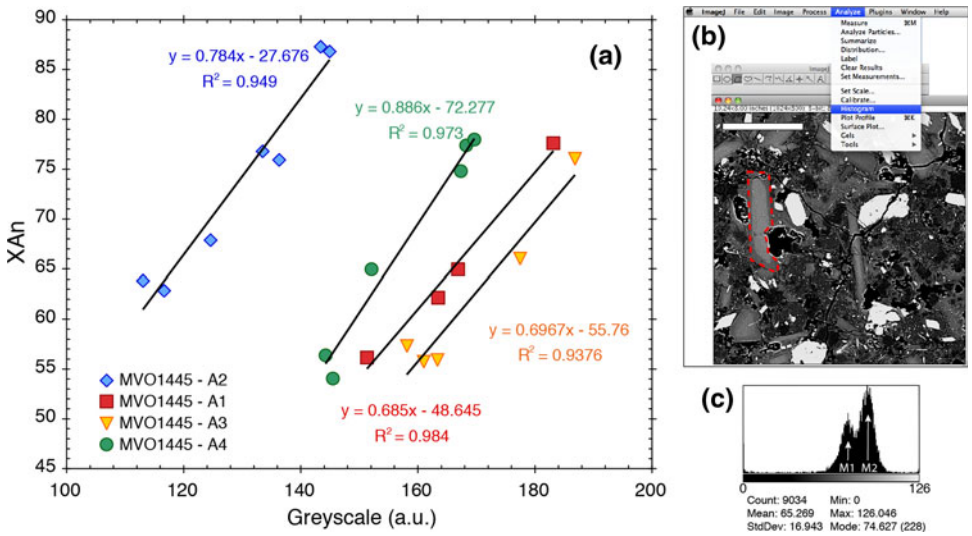

Fig. 2 **a** Typical greyscale calibrations for anorthite content (X_{An}). Each set of *symbols* shows the calibration for a different image. *a.u.* arbitrary units. **b** Screen capture from ImageJ software (Rasband 1997–2011) showing the approach of highlighting an individual crystal and extracting a histogram from the calibrated image. **c** ImageJ histogram or X_{An} distribution extracted from the crystal shown in (**b**) (colour figure online)

BSE intensity is closely related to the average atomic number of the sample; regions with higher atomic number give brighter BSE intensity. Ginibre et al. (2002) demonstrated that for plagioclase, BSE intensity correlates well with X_{An} since the dominant effect on atomic number of the plagioclase is the CaAl-NaSi variation and the total wt% of minor elements is very small. Each BSE image was therefore calibrated for X_{An} with between 4 and 7 electron microprobe analyses using a JEOL-JSM-8600 electron microprobe at the RLAHA, University of Oxford. Operating conditions were a 15-kV accelerating voltage, 10 nA beam current, 1–2 μm beam diameter, and typically 30 s peak counting time. Primary standards used were wollastonite (for Si, Ca), haematite (Fe), albite (Na), periclase (Mg), orthoclase (K) and rutile (Ti).

Image processing methods

For each image, we used ImageJ (Rasband 1997–2011) to extract the average BSE intensity for each spot analysed by electron microprobe. The plagioclase compositions analysed show good positive linear correlations of X_{An} with BSE intensity, with R^2 typically >0.9 (Table 2; Fig. 2). We then used the 'Calibrate Image' function within ImageJ to convert the whole image to 'X_{An}'. For each calibrated image, we then used ImageJ to outline the margins of each plagioclase crystal and analyse its greyscale variation as a histogram (Fig. 2). For the andesite, between 16 and 43 crystals were analysed in each of 14 images at 170× magnification, yielding a set of 342 greyscale histograms. For the mafic inclusion, between 21 and 65 crystals were analysed in each of 7 images at 90× magnification, giving 276 individual greyscale histograms. These histograms were processed individually. We also produced 21 'bulk' histograms containing the summed individual histograms from each image, which were also processed and compared with the individual fits summed after processing.

Image artefacts

Clearly, calibration of a whole image to anorthite content will be meaningless for components other than plagioclase in the image. Bright BSE intensity mineral inclusions (e.g. pyroxene or oxides) are seen in the histograms as obvious blips at very high greyscale intensity (typically correlating to >100 mol% anorthite after calibration) and were therefore easily excluded from the histograms. This artefact was more apparent for the mafic inclusion sample, because numerous small pyroxene crystals commonly occur near the margins of plagioclase crystals. Obvious cracks, vesicles or polishing pits (anomalously dark features in BSE images) resulted in anomalously low greyscale intensity features. Sometimes these correlated to <0 mol% anorthite after calibration, in which case they could be easily excluded from the histograms. More commonly, however, they corresponded to low anorthite contents at around $An_{20–30}$. The result of this is to give a slight left-handed (negative) skew to the histograms. This was less easily corrected for and cannot in principle be distinguished from the effect of low-X_{An} overgrowths, except for the fact that the most sodic plagioclase microlite reported is $\sim An_{45}$, so anything more sodic than this is probably an artefact. We truncated all the X_{An} distributions at 30 mol% Anorthite and consider that the overall effect of these artefacts is small and does not materially affect our conclusions.

Data fitting methods

Each X_{An} distribution was processed and fitted in the same way using the IgorPro software package, whether for an individual crystal, summed crystals ('bulk histogram') or synthetic crystal. We attempted to fit the data with each of one Gaussian, two Gaussians and a skewed (exponentially modified Gaussian) distribution. The Gaussian nature of the curves is derived from the noise in the original BSE images. Thus, a good single Gaussian fit indicates a crystal that is essentially unzoned (within the noise of the image), while a good 2-peak fit indicates a crystal that has a single-composition core and a different, single-composition rim. A good fit by the skewed Gaussian, or a single Gaussian with large standard deviation, could indicate minor compositional zoning (e.g. a thin sodic rim could produce a skewed curve with a slight left-hand, low-X_{An} tail).

Significance Testing and Fit Quality Checks

After fitting, we calculated two quantities to test for the significance of the 2-peak fit. Firstly, we calculated the resolution, R_s (following peak identification procedures in gas chromatography studies, e.g., Snyder et al. 1997). This is a measure of the degree of separation of two normally distributed (Gaussian) peaks and is proportional to the distance between the means, relative to the widths of the distributions:

$$R_s = \frac{1.18(M_2 - M_1)}{W_1 + W_2} \quad (1)$$

where M_i is the mean (peak) X_{An} value and W_i is the full width at half maximum height (FWHM) of curve i (we define peak 2 as that with higher X_{An}). We retained only fits with $R_s \geq 0.4$ because errors started to become significant after this point for the synthetic crystals (see later). Resolution does *not* take into account variations in relative peak height; therefore, two sets of peaks with the same M and W but different relative weightings will not be distinguishable using R_s (Fig. 3).

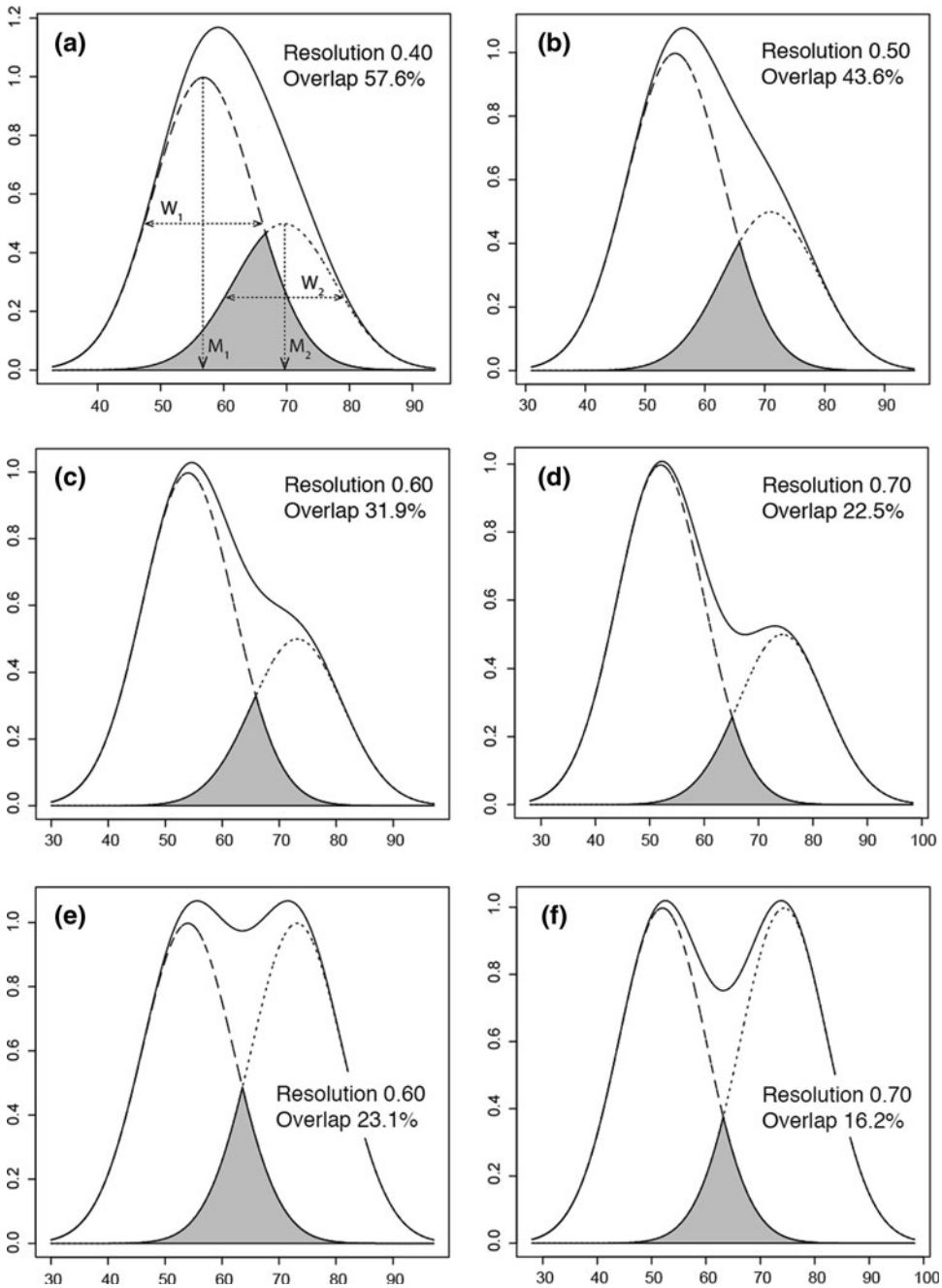

Fig. 3 Synthetic resolution curves for $R_s > 0.4$, for pairs of overlapping Gaussian curves with area ratio of 2:1 (parts **a**–**d**) or 1:1 (**e**, **f**). The individual curves are shown by the *short-dashed* and *long-dashed lines*. The overall distribution is given by the *solid curve*. The overlapping region is shown in *grey*; % overlap quoted is for the smaller curve (i.e. maximum overlap). In (**a**), *dotted lines* show the mean value (M_i) and full width at half maximum (W_i) as described in Eq. (1)

We therefore used an additional constraint: the proportion of one curve overlapped by the other. This was calculated using a simple integration routine written using the statistical package R (R Development Core Team 2010). As expected, the % overlap (of the smaller peak) tends to be smaller for distributions with higher R_s (Fig. 3). Fits with ≥60 % overlap of the smaller peak were rejected, even if these still had relatively high R_s, again because for the synthetic X_{An} distributions, errors started to become significant for overlaps >60 % (see later). Two-peak fits where the data were matched equally well or better (within ≤5 % of the χ^2 value) by an exponentially modified (skewed) Gaussian or where the peak X_{An} was outside realistic bounds (<An_{45} or >An_{90}) were not retained. Finally, the standard deviation (or width) of a peak can be greater than that of the original image noise (typically 4–8 mol%) if there is smooth compositional zoning in the crystal, but should not be significantly less. We therefore also rejected fits where the standard deviation of either peak was either <approx 3.5 mol% or >11 mol%; these were usually clearly spurious on visual inspection. We are confident that these data quality checks resulted in only

significant and meaningful 2-peak fits being counted. Finally, we calculated the area ratio of the two peaks, A_1/A_2, in order to obtain an estimate of the relative importance of each of the two overlapping Gaussian curves to the total distribution.

Results—synthetic X_{An} distributions

We produced and analysed three synthetic crystal geometries, all with an An-rich core and An-poor rim, and each with a range of compositional contrast between core and rim (Fig. 4): (A) large core (79.7 % area); (B) intermediate core (40 % area); (C) small core (8.2 % area). For each, we tested high-noise examples (standard deviation of applied noise = 8 mol%) and low-noise examples (standard deviation = 4 mol%). In each example, the core is varied in composition from An_{68} to An_{72} and the rim from An_{50} to An_{60}, such that the total compositional contrast between core and rim (denoted ΔX) varies by up to 4–22 mol% X_{An}. The full data set is given in Appendix 1 in ESM.

In all cases, the peak X_{An} and the relative areas of the two peaks were retrieved very well until ΔX is approximately $\leq$1–2 times the standard deviation of the noise, but this depends on the relative size variation of the core and rim (see below). At smaller ΔX, errors increase and can become very significant (Figs. 5, 6). However, as a rule of thumb, errors are very small for $\Delta X \geq 1.5\ \sigma$. For an example with core An_{70} and rim An_{56} (typical values for the andesite microlites; $\Delta X = 14$), deviations between known and calculated relative peak area for the cores are 0.1–4 % relative (case A), 0.1–37 % relative (case C) and 1.4–10 % relative (case B), with the larger value for the high-noise version in each case. Equivalent deviations for the rims are 0–1.1 % relative (case A), 0–0.4 % relative (case B), and 0–0.3 % relative (case C; see Table 3 for details). The ratio of the deviations between known and calculated core and rim areas is equivalent to the ratios of the areas—in other words, the error on the calculated area would be identical for cores and rims that were the same size and is most significant for a very small core or rim. Errors therefore increase with decreasing ΔX, decreasing relative peak area and increasing image noise. Peak X_{An} values were generally retrieved most successfully, with errors typically $\ll$1 % relative.

Results—andesite X_{An} distributions

Individual crystal X_{An} distributions

Individual X_{An} distributions were extracted and fitted from 342 plagioclase crystals in the andesite groundmass. Many of the distributions are approximately symmetrical or have a slight left-hand skew, but several clearly have two underlying components (see examples in Fig. 7). 54 of the distributions resulted in significant 2-peak fits (as quantified using the resolution and % overlap indicators, see earlier). The remainder had a better fit to either a single Gaussian (indicating an essentially unzoned or only very weakly zoned crystal) or, less commonly, to an exponentially modified Gaussian.

Of the single Gaussian fits, the average peak X_{An} value was $An_{61.3}$ (1σ = 5.8 mol% An) with average FWHM of 20.8 mol% X_{An} (n = 288; Tables 2, 3). This is consistent with the compositions of plagioclase microlites as determined in previous studies (e.g. Murphy et al. 2000; Couch et al. 2003). There is a weak positive relationship between crystal size (as determined by pixel count) and peak location, with the largest crystals tending to have relatively An-rich peak positions at around An_{60}–An_{65} (Fig. 8).

Of the 2-peak fits, the average peak X_{An} values were $An_{56.1}$ (1 σ 4.3 mol% An; average FWHM 17.7 mol% An) and $An_{71.6}$ (1 σ 4.4 mol% An; average FWHM 15.4 mol% An; n = 54; see Tables 2, 3). The average area ratio of peak 1 (sodic) to peak 2 (calcic) is $\sim$1.8, but this value is highly variable (1 σ 1.7; min 0.1; max 4.6). The amount of overlap with the smaller peak in these retained fits is 14–60 % (average 40 %). Average resolution (R_s) is 0.52. Between 8 and 61 % of all the crystals analysed were fit equally well or better by a skewed Gaussian (average 34 %).

The proportion of 2-peak fits retained is 15.8 %, but this proportion is highly variable between images (minimum 3.2 %, maximum 34.8 %). We used the proportion of 2-peak fits retained in each image, together with the average area ratio of peak 1:peak 2, to calculate the total *area* contribution of the An-rich component (peak 2) to each plagioclase population (where A = area):

$$\text{Total } pk2 \text{ contribution} = \frac{A_{pk2}}{\left(A_{pk2} + A_{pk1}\right)} \times \%\text{ of 2-peak fits retained}$$

For example, an image may contain 20 % 2-peak fits. Of these, the average area proportion of the An-rich peak is 30 %. Therefore, the total contribution of those An-rich peaks to the plagioclase population in that image is $0.2 \times 0.3 = 6$ %. Using this method, we calculated the total contribution of the An-rich component to be 0.7–18.9 % of the plagioclase population in each image (average 8.0 %).

Summated bulk X_{An} distributions

The bulk histograms produced by summing all the individual X_{An} distributions were also processed and analysed. The bulk histograms range from subtle two-component distributions to apparently symmetric, unimodal

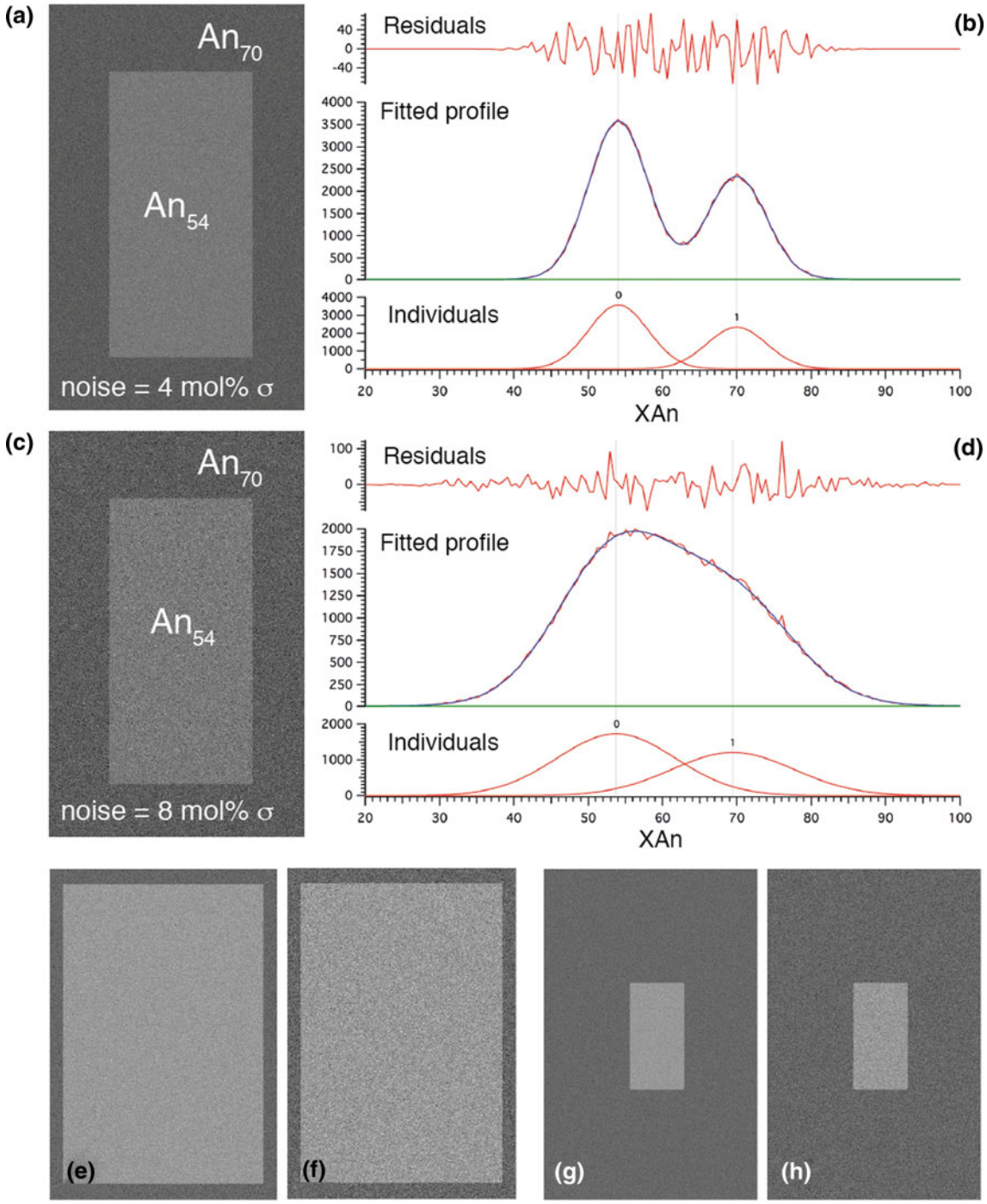

Fig. 4 Synthetic 'crystals' used to evaluate the likely uncertainties of the method. **a** Intermediate sized core (40 % of total area), with low noise (standard deviation, $\sigma = 4$ mol%). **b** IgorPro fitting results from (**a**) showing the two individual peaks relating to the core and rim, fitted profile and residuals. **c**, **d** As in (**a**, **b**) but for the high-noise case ($\sigma = 8$ mol%). **e**, **f** Low- and high-noise images showing the large core crystal (80 % of total area). **g**, **h** Low- and high-noise images showing the small core crystal (8 % of total area). In all examples $\Delta X = 16$ mol%

distributions (Fig. 9). Consequently, only three of the fourteen images examined gave bulk distributions with significant 2-peak fits with $R_s > 0.4$ and with <60 % overlap. For the retained fits, the peak X_{An} values are retrieved fairly well (by comparison with the average peak locations for all the individual histograms). However, the total contribution of the An-rich component does not correlate well with the average of the individual results and results in bulk distributions with approximately twice the estimate of total peak 2 contribution.

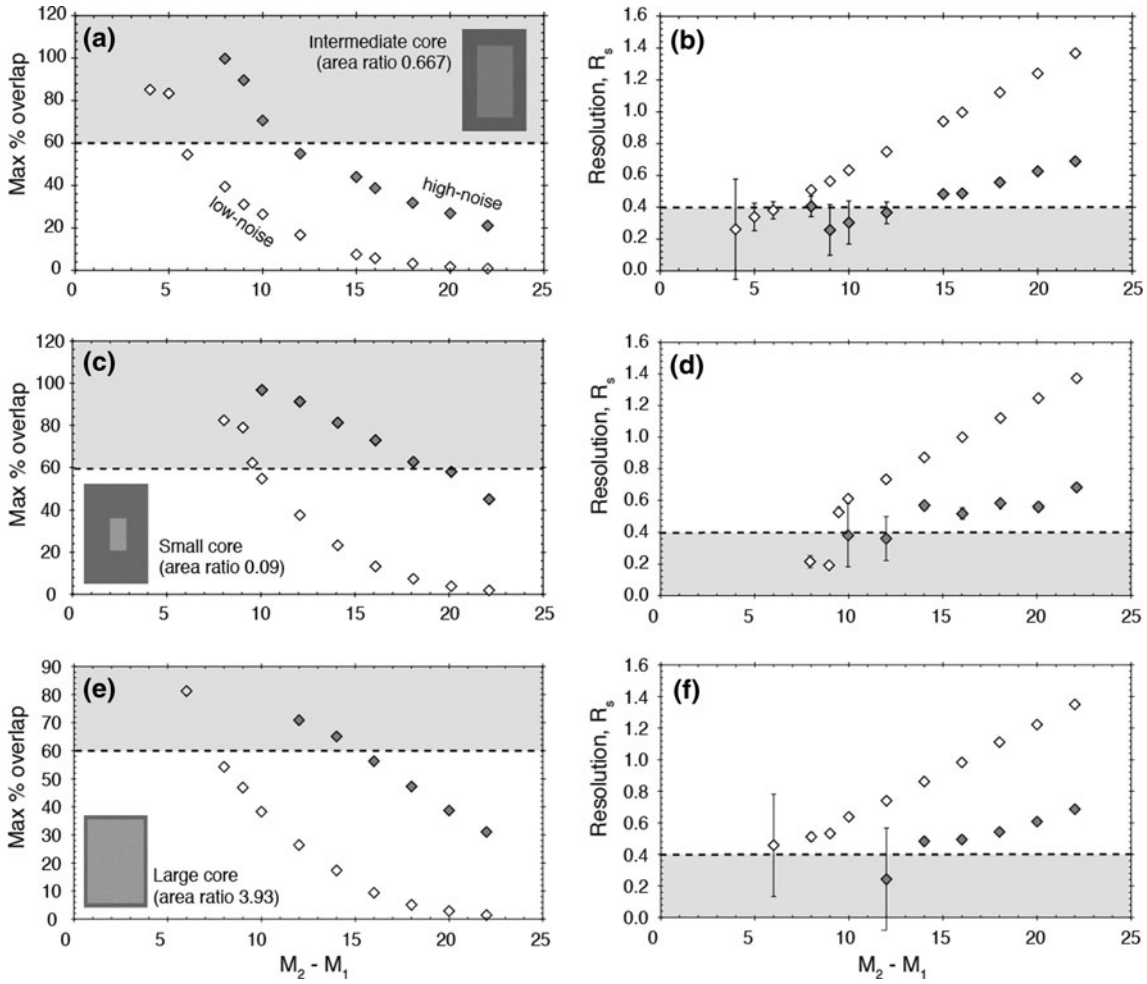

Fig. 5 Results of greyscale distribution analysis for three synthetic crystal cases as described in the text. *Grey diamonds*: low-noise case ($\sigma = 4$ mol%); *open diamonds*: high-noise case ($\sigma = 8$ mol%). The *left-hand* panels show the % overlap of the smaller peak, and the *right-hand* panels show the resolution, as a function of the separation of the two peaks ($M_2 - M_1$). The limits for retaining a good fit were max overlap <60 % and $R_s > 0.4$; therefore points within the *greyed-out boxes* would not be retained. Area ratios quoted are core: rim

Results—mafic inclusion X_{An} distributions

Individual crystal X_{An} distributions

Individual X_{An} distributions were extracted and fitted from 276 plagioclase crystals in the mafic inclusion sample. Typically, these histograms appear approximately symmetrical or have a slight left-hand skew (long left-hand tail, see Fig. 10). Only 20 distributions resulted in significant 2-peak fits. The remainder were fit better either by a single Gaussian or commonly by an exponentially modified Gaussian. Of the single Gaussian fits, the average peak X_{An} value was $An_{70.7}$ ($1\sigma = 4.4$ mol% An) with average FWHM of 21.8 mol% X_{An} ($n = 256$). This is consistent with the compositions of mafic inclusion plagioclase as determined in previous studies (e.g. Murphy et al. 2000; Humphreys et al. 2009a). For crystals over ~3000 pixels in size (~55 μm side length), there is a slight positive correlation between peak location and crystal size, with the largest crystals giving fitted peak compositions of ~An_{80} (Fig. 8).

Of the 2-peak fits, the average peak X_{An} values were $An_{60.2}$ (1 σ 6.0 mol% An; average FWHM 17.2 mol% An) and $An_{76.2}$ (1 σ 5.8 mol% An; average FWHM 16.5 mol% An; $n = 20$; see Tables 2, 4). The average area ratio of peak 1 (sodic) to peak 2 (calcic) is ~0.7, that is, much smaller than for the andesite crystals, but this value is again quite variable (1 σ 0.6; min 0.2; max 2.9). The amount of overlap with the smaller peak in these retained fits is 20–56 % (average 37 %). The total contribution of the more An-rich component in the mafic inclusion plagioclases is 65 %. Average resolution (R_s) = 0.57, and 48–66 % of the crystals in each image were fit equally well or better by a skewed Gaussian (average 53 %, Tables 2, 4).

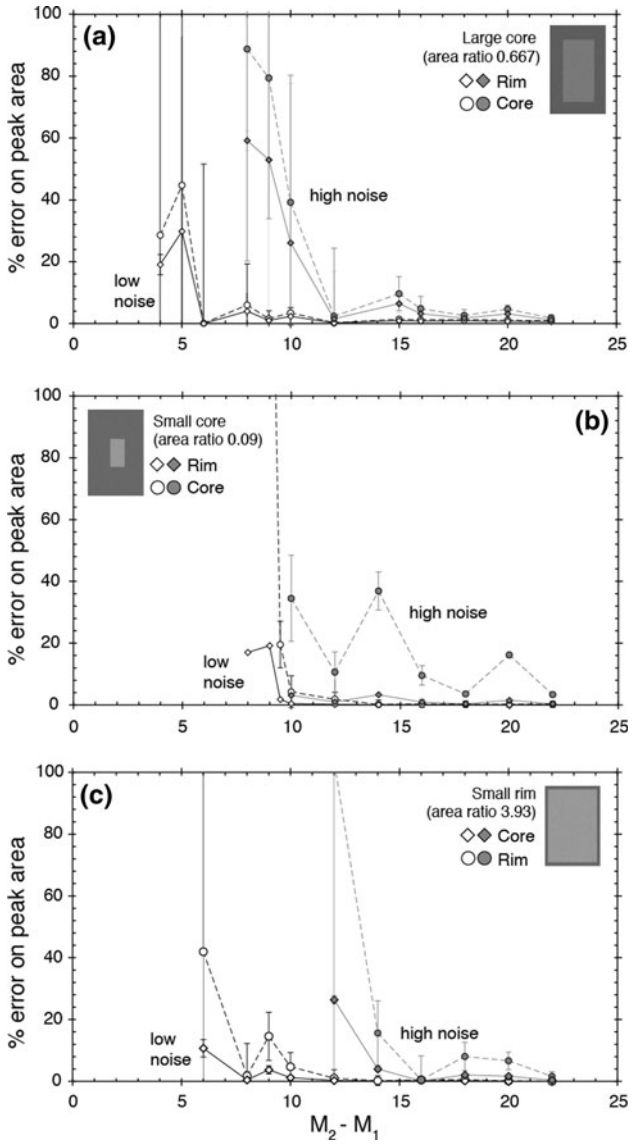

Fig. 6 Results of greyscale distribution analysis for three synthetic crystal cases as described in the text. Each plot shows the error on the calculated peak area relative to the known value. *Dark symbols* show the high-noise case; *open symbols* show the low-noise case

Summated bulk X_{An} distributions

The bulk X_{An} distributions for mafic inclusion plagioclase are typically left-hand skewed curves with the main peak at $\sim An_{70}$–An_{75}, and without any clear second (An-poor) component (Fig. 11). R_s values range from 0.26 to 0.31, with maximum overlaps of 62–98 %; hence, none of the two-peak fits was retained.

Melts modelling

As an independent check on the shape of the X_{An} distribution produced under known conditions, we used MELTS (Ghiorso and Sack, 1995) to predict the variation of X_{An} during crystallisation of a mafic liquid. We assumed that the bulk compositions of mafic inclusions represent true magmatic liquids (i.e. only minimal hybridisation has occurred; for a discussion see Plail et al. 2012) and that crystallisation occurs by closed-system, isobaric fractional crystallisation within the andesite storage region. We used the most mafic composition of the Phase III mafic inclusions presented by Barclay et al. (2010) as the initial melt and assumed $P = 200$ MPa (based on H_2O contents of melt inclusions in the andesite, Humphreys et al. 2009b) and an oxygen fugacity of QFM + 2 (see Table 5). We simulated fractional crystallisation from the liquidus with a range of volatile contents (0–4 wt% H_2O and 0–1 wt% CO_2) and attempted to match the natural observations (plagioclase An_{90}–An_{55}; clinopyroxene ± orthopyroxene + magnetite ± ilmenite; 10–30 % SiO_2-rich residual glass; maximum crystallisation temperatures of approximately 1,150 °C, based on the upper estimates of magmatic temperatures derived from 2-pyroxene geothermometry, Humphreys et al. 2009a, although these temperatures may represent disequilibrium conditions).

The anhydrous run (*A*) was unable to match the most An-rich plagioclase compositions observed, reaching $\sim An_{82}$ at the liquidus and requiring extremely high temperatures (>1,250 °C). This is unreasonable given temperature estimates of ~1,150 °C, and in any case, the mafic inclusions are invariably vesicular. The magma has only 4.5 % melt remaining at 850 °C, with almost pure albite ($An_{1.5}$) predicted to be in equilibrium with the remaining liquid (Table 5). The modal assemblage was plag + opx + mt + cpx + qz; at 850 °C, the residual liquid had 79 wt% SiO_2. In comparison, runs with increasing amounts of H_2O in the starting melt produced higher initial anorthite contents and reduced the extent to which the plagioclase became more sodic with fractional crystallisation. For example, with 2 wt% H_2O in the initial melt, the initial composition is An_{88} at 1,150 °C, reaching An_{41} at 850 °C (Table 5) with 26 % liquid remaining at 67 wt% SiO_2; the crystallisation products are plag + cpx + opx + mt. With 4 wt% H_2O in the initial liquid, the plagioclase composition is An_{90} at 1,062 °C (clinopyroxene crystallises first from the liquidus at 1,096 °C), reaching An_{38} at 850 °C (with 30 % liquid still remaining), but plagioclase crystallises late, after clinopyroxene and magnetite (Table 5) and the residual liquid has only 64 wt% SiO_2. The absence of predicted stable amphibole from the modelling contrasts with its occurrence in some of the inclusions; this may be related to changes in crystallisation sequences due to rapid undercooling (Blundy and Sparks 1992).

In comparison with fractional crystallisation, the effect of equilibrium crystallisation is to reduce the degree of X_{An}

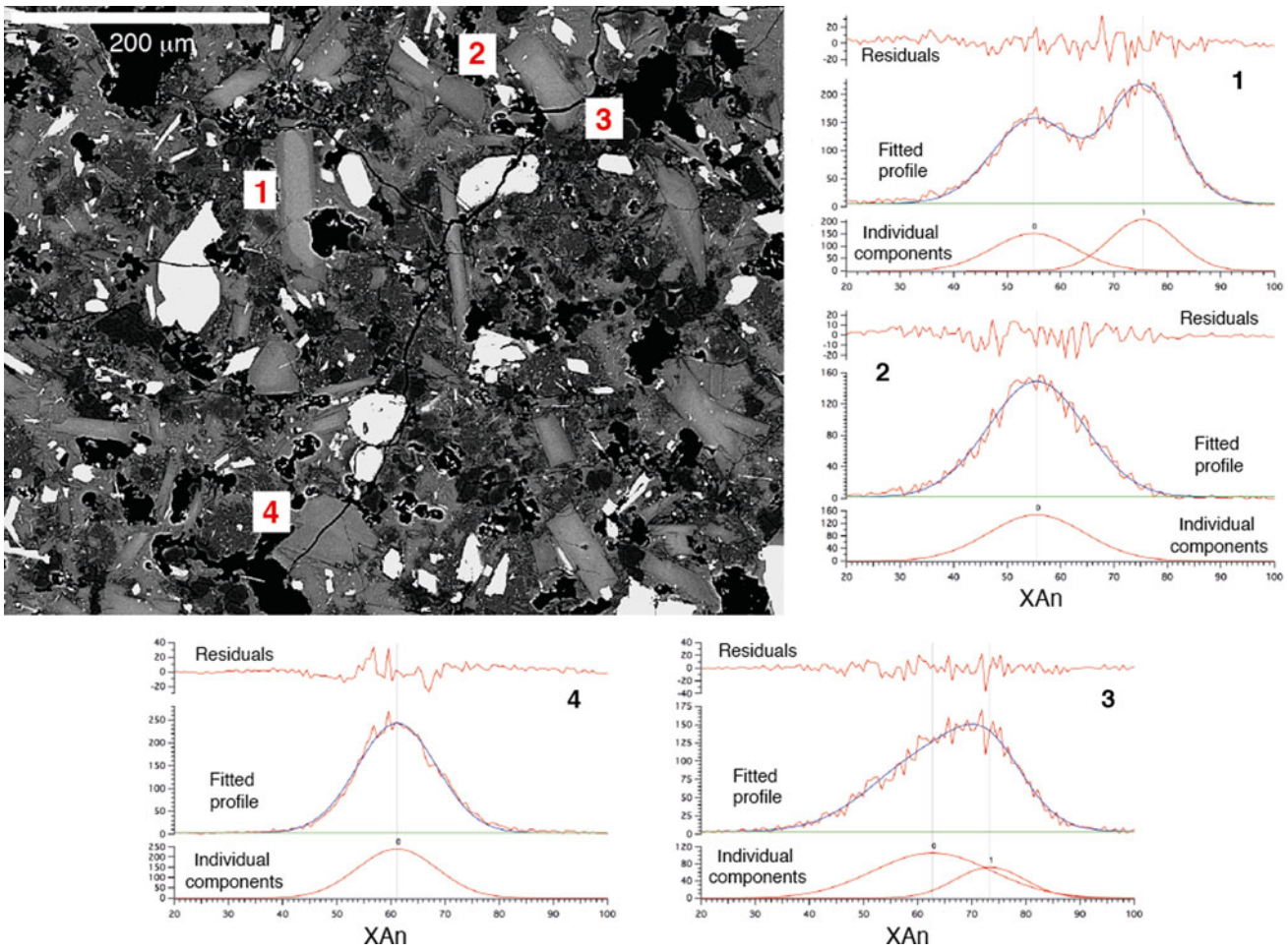

Fig. 7 Typical X_{An} distributions for individual crystals from the andesite. The main images show a back-scattered electron image of part of the andesite groundmass. Four crystals are labelled which show the range of X_{An} distributions observed. (*1*) Clear two-component distribution with calcic core ($An_{75.4}$) and sodic rim ($An_{55.0}$). $R_s = 0.69$, maximum overlap = 15.2 %. (*2*) and (*4*) Single-component distributions with $An_{55.5}$ and $An_{61.1}$, respectively. (*3*) Two-component distribution with core $An_{73.3}$ and rim $An_{62.5}$, but doesn't pass both criteria for being retained ($R_s = 0.59$ but maximum overlap = 83.7 %)

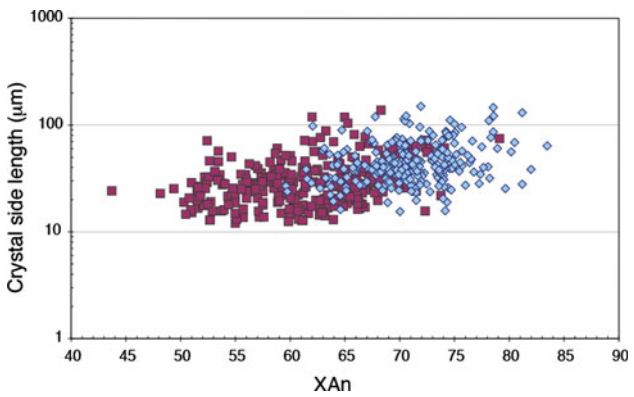

Fig. 8 Variation of peak location (X_{An}) with crystal area (determined by pixel count) for the single-component distributions. *Red squares*: plagioclase from the andesite. *Blue diamonds*: plagioclase from the mafic inclusion sample. There is a positive relationship between composition and size, with the largest crystals showing the most An-rich compositions

variation, to decrease the amount of melt remaining at 850 °C, and to produce less evolved residual liquids. The addition of modest amounts of CO_2 appears to have little effect on the plagioclase composition or amount of glass remaining (Table 5). We therefore suggest that the mafic inclusions may have contained ~2 wt% H_2O prior to mixing and cannot rule out that the inclusions also contained up to ~1 wt% CO_2. We also infer that, because intruding mafic magmas with the highest volatile contents are likely to have a lot of residual melt when they cool to the ambient temperature of the host magma, these magmas are least likely to be preserved as mafic inclusions. The abundance of residual melt would mean that these melts have lower viscosity (e.g. Costa 2005) and this would make disaggregation of these inclusions easier (Clynne 1999), as might the internal pressure produced by strong vesiculation.

Bulk anorthite distributions for the run with 2 wt% H_2O were produced by dividing the MELTS output into bins of

Table 2 Calibrations used for conversion of BSE images to X_{An}, and the number of crystals identified with good 2-component X_{An} distributions

Andesite image name	Image calibration	R^2	No. crystals analysed	2-peak fit	1-peak fit	% 2-peak fits	% porosity in image
MVO1445-A1	$X_{An} = 0.685x - 48.645$	0.98	29	6	23	20.7	14.1
MVO1445-A2	$X_{An} = 0.784x - 27.676$	0.95	24	4	20	16.7	13.5
MVO1445-A3	$X_{An} = 0.697x - 55.760$	0.94	21	5	16	23.8	16.3
MVO1445-B1	$X_{An} = 0.750x - 58.214$	0.90	20	2	18	10.0	11.9
MVO1445-B2	$X_{An} = 1.619x - 219.15$	0.86	24	3	21	12.5	23.3
MVO1445-B3	$X_{An} = 0.774x - 61.662$	0.98	20	6	14	30.0	13.4
MVO1445-B4	$X_{An} = 0.752x - 50.526$	0.92	23	8	15	34.8	12.4
MVO1445-C2	$X_{An} = 2.441x - 206.18$	0.94	35	3	32	8.6	14.5
MVO1445-C3	$X_{An} = 2.372x - 180.63$	0.95	20	2	18	10.0	12.8
MVO1445-C4	$X_{An} = 1.596x - 86.036$	0.94	43	2	41	4.7	6.7
MVO1445-C6	$X_{An} = 2.330x - 137.37$	0.92	17	3	14	17.6	17.2
MVO1445-D1	$X_{An} = 1.939x - 187.11$	0.99	31	1	30	3.2	9.5
MVO1445-D2	$X_{An} = 1.684x - 147.74$	0.95	19	5	14	26.3	10.4
MVO1445-D3	$X_{An} = 1.112x - 117.49$	0.88	16	4	12	25.0	12.2
Total			342	54	288	17.4	
Mafic inclusion image name	Image calibration	R^2	No. crystals analysed	2-peak fit	1-peak fit	% 2-peak fits	
MVO1448-A1	$X_{An} = 1.180x - 86.615$	0.89	33	1	32	3.0	
MVO1448-A3	$X_{An} = 1.665x - 112.87$	0.99	30	2	28	6.7	
MVO1448-B1	$X_{An} = 1.409x - 100.18$	0.90	36	3	33	8.3	
MVO1448-D2	$X_{An} = 2.246x - 234.79$	0.94	21	0	21	0.0	
MVO1448-D3	$X_{An} = 1.483x - 122.19$	0.72	45	5	40	11.1	
MVO1448-D4	$X_{An} = 1.323x - 108.5$	0.77	46	2	44	4.3	
MVO1448-D5	$X_{An} = 1.738x - 148.67$	0.995	65	7	58	10.8	
Total			276	20	256	7.8	

'x' = BSE greyscale intensity. % porosity in each image is estimated by thresholding using ImageJ

2.5–5 % anorthite and calculating the total amount of plagioclase crystallisation that occurred while the equilibrium X_{An} was within each bin. The result is a unimodal histogram with a long tail to low X_{An} and peak at $\sim An_{80–90}$ (Fig. 12). This corresponds reasonably well with the shape of the bulk anorthite distributions produced from the BSE images of the mafic inclusion. In comparison, equilibrium crystallisation led to approximately constant amounts of crystallisation in each bin.

The key differences between the modelled and analysed X_{An} distributions are the degree of skewness (greater in the modelled distribution) and the peak X_{An} value, which is slightly higher for the modelled distribution. The possible causes of these discrepancies are (a) the presence of noise in the processed distributions, (b) small mismatches in the starting conditions or melt composition for the modelled distributions, (c) the possibility of strong disequilibrium during crystallisation of the natural samples, and (d) that the calculated X_{An} distribution is based on relative volume calculations while those from image processing are based on relative area (see later for more discussion of area-volume issues). The key point is that a left-hand skewed distribution is produced in both cases, with similar peak X_{An} values.

Interpretation of X_{An} distributions

Previous studies have shown that the very anorthite-rich plagioclase microlite compositions that are commonly observed in andesite from Soufrière Hills Volcano cannot have crystallised in equilibrium with the relatively cool, silicic melt ($\sim$850 °C, $\sim$78 wt% SiO_2). Although it is possible to produce fairly high X_{An} by crystallising at high temperatures and pH_2O (e.g. Couch et al. 2003), Humphreys et al. (2009a) argued that the high FeO and MgO contents of such microlites could be achieved by crystallising from a melt that was also enriched in Fe and Mg, although strong disequilibrium growth would also be expected to enhance Fe and Mg partitioning. Given the good compositional correspondence between the microlites

Table 3 Results of 2-component fits to andesite groundmass plagioclase

Image	Crystal	M1	SD1	A1	W1	M2	SD2	A2	W2	Area ratio	Max % overlap	Total area (pixels)	Resolution (Rs)	M2-M1
MVO1445-A1	B	55.3	7.03	369	16.6	68.7	5.90	122	13.9	3.0	51.5	491	0.490	13.4
	K	55.0	7.67	2,912	18.1	75.4	6.30	3,295	14.8	0.9	15.2	6,207	0.694	20.4
	L	54.2	7.37	454	17.4	70.2	5.38	140	12.7	3.2	39.5	595	0.597	16.0
	N	55.5	5.12	140	12.1	68.6	7.00	372	16.5	0.4	47.2	512	0.513	13.1
	W	56.6	8.70	2,953	20.5	72.0	6.57	1,582	15.5	1.9	44.3	4,535	0.477	15.3
	AD	53.6	7.47	434	17.6	70.2	4.51	42	10.6	10.4	59.9	476	0.657	16.6
MVO1445-A2	B	62.7	6.17	484	14.5	75.3	5.69	365	13.4	1.3	33.3	848	0.504	12.6
	D	64.6	6.79	822	16.0	77.1	6.00	667	14.1	1.2	36.5	1,488	0.465	12.5
	K	61.2	7.70	2,234	18.1	76.8	5.80	2,227	13.7	1.0	24.5	4,461	0.549	15.6
	Q	65.3	7.66	5,268	18.0	76.5	5.23	4,773	12.3	1.1	39.9	10,041	0.412	11.2
MVO1445-A3	C	62.5	6.67	740	15.7	76.3	5.85	412	13.8	1.8	36.3	1,153	0.524	13.8
	J	55.7	6.81	383	16.0	72.1	4.93	111	11.6	3.4	32.0	494	0.661	16.3
	N	53.4	6.78	285	16.0	69.1	6.15	583	14.5	0.5	30.7	868	0.575	15.6
	Q	50.7	5.62	886	13.2	64.7	7.33	1,492	17.3	0.6	37.1	2,377	0.513	14.0
	W	58.1	8.21	663	19.3	75.0	4.97	137	11.7	4.8	48.5	800	0.611	17.0
MVO1445-B1	H	57.3	6.28	1,617	14.8	68.9	5.17	979	12.2	1.7	42.9	2,596	0.480	11.6
	T	61.1	7.40	3,026	17.4	73.1	5.91	1,455	13.9	2.1	53.9	4,481	0.427	12.0
MVO1445-B2	K	55.3	9.33	5,446	22.0	74.2	7.59	1,315	17.9	4.1	52.9	6,760	0.529	18.9
	O	50.3	8.80	356	20.7	66.5	6.28	163	14.8	2.2	43.5	519	0.509	16.2
	R	51.2	9.81	2,375	23.1	70.2	6.77	1,623	15.9	1.5	31.3	3,998	0.542	18.9
MVO1445-B3	B	57.7	8.13	1,511	19.2	72.0	5.55	637	13.1	2.4	48.2	2,148	0.494	14.2
	D	58.3	7.67	1,076	18.1	74.5	9.22	1,192	21.7	0.9	35.7	2,267	0.454	16.1
	E	62.8	8.80	5,917	20.7	78.0	6.75	5,987	15.9	1.0	32.5	11,903	0.465	15.2
	Q	54.7	8.52	5,362	20.1	70.3	7.66	5,287	18.0	1.0	33.5	10,649	0.459	15.7
	R	54.7	8.00	678	18.8	73.2	6.42	262	15.1	2.6	32.7	939	0.610	18.5
	T	53.0	7.90	322	18.6	76.1	8.09	895	19.0	0.4	24.1	1,217	0.685	23.1
MVO1445-B4	A	53.6	8.65	4,053	20.4	75.0	7.13	4,241	16.8	1.0	17.7	8,294	0.644	21.4
	G	54.4	8.36	1,007	19.7	72.3	7.52	792	17.7	1.3	29.5	1,799	0.534	17.9
	H	53.6	8.07	2,747	19.0	76.9	7.37	2,442	17.4	1.1	13.8	5,189	0.719	23.4
	I	54.2	9.28	1,314	21.8	75.7	6.33	283	14.9	4.6	39.2	1,597	0.652	21.4
	L	49.9	8.10	777	19.1	67.5	8.64	2,225	20.3	0.3	47.3	3,002	0.500	17.6
	M	55.3	7.90	754	18.6	73.8	7.57	568	17.8	1.3	26.8	1,321	0.567	18.5
	R	49.5	7.85	1,055	18.5	66.76	9.54	3,827	22.5	0.3	59.6	4,882	0.471	17.3
	V	51.9	6.16	516	14.5	71.2	8.88	2,796	20.9	0.2	48.5	3,311	0.612	19.4
MVO1445-C2	AC	53.0	8.73	154	20.6	78.2	7.94	2,153	18.7	0.07	35.2	2,307	0.720	25.3
	S	53.3	6.71	399	15.8	66.6	6.06	358	14.3	1.1	31.7	756	0.492	13.3
	L	55.8	5.72	475	13.5	66.9	6.53	803	15.4	0.6	47.6	1,278	0.431	11.1
MVO1445-C3	E	52.3	6.88	2,049	16.2	67.5	9.12	5,200	21.5	0.4	56.1	7,248	0.450	15.2
	Q	61.7	8.57	5,602	20.2	74.5	6.54	5,339	15.4	1.0	40.3	10,941	0.402	12.8
MVO1445-C4	A	66.3	5.46	11,986	12.9	75.7	3.76	7,290	8.9	1.6	40.7	19,276	0.483	9.4
	AQ	60.0	3.87	470	9.1	69.8	4.71	2,133	11.1	0.2	52.0	2,603	0.545	9.8
MVO1445-C6	F	51.6	7.03	1,997	16.5	63.9	6.70	2,386	15.8	0.8	55.6	4,383	0.427	12.4
	L	49.7	4.76	989	11.2	58.2	3.85	344	9.1	2.9	40.0	1,334	0.464	8.4
	A	60.9	7.80	4,383	18.4	73.2	5.75	2,469	13.5	1.8	49.7	6,851	0.432	12.3
MVO1445-D1	A	53.3	11.09	1,857	26.1	71.5	9.20	2,384	21.7	0.8	40.6	4,240	0.426	18.2

Table 3 continued

Image	Crystal	M1	SD1	A1	W1	M2	SD2	A2	W2	Area ratio	Max % overlap	Total area (pixels)	Resolution (Rs)	M2-M1
MVO1445-D2	A	58.0	9.81	10,363	23.1	73.9	7.38	6,811	17.4	1.5	44.4	17,174	0.440	15.9
	D	58.7	6.60	1,095	15.5	69.3	4.18	385	9.8	2.8	58.5	1,480	0.467	10.6
	G	49.7	5.93	632	14.0	60.0	4.67	395	11.0	1.6	42.3	1,027	0.464	10.4
	I	51.5	8.69	1,238	20.5	66.6	8.98	773	21.1	1.6	48.8	2,011	0.403	15.0
	T	56.7	8.33	2,893	19.6	70.0	7.34	2,099	17.3	1.4	46.6	4,992	0.404	13.3
MVO1445-D3	A	58.6	8.14	5,849	19.2	71.8	5.89	5,740	13.9	1.0	34.1	11,589	0.449	13.3
	C	57.0	6.71	1,947	15.8	75.4	5.85	523	13.8	3.7	27.1	2,470	0.697	18.4
	K	62.8	7.74	468	18.2	76.7	4.40	133	10.4	3.5	52.9	601	0.542	13.8
	P	55.8	5.83	369	13.7	72.3	8.79	481	20.7	0.8	29.6	850	0.537	16.5
Average		56.1				71.6				1.8				
SD		4.3				4.4				1.7				

M X_{An} location of peak, *SD* standard deviation of peak, *A* area under peak, *W* full width at half maximum, Area ratio = A1/A2

and plagioclase from mafic inclusions, the implication is that the very An-rich microlites are probably scattered into the andesite by mechanical disaggregation of mafic inclusions (Humphreys et al. 2009a). It is this mafic-derived component that we interpret to form the An-rich component of the two-peak fits in the andesite plagioclase.

To summarise our results: approximately 16 % of small plagioclase crystals from the andesite groundmass have X_{An} distributions with two significant components, one at $\sim An_{56}$ and one at $\sim An_{72}$. The An-poor peak (M1) is dominant in area relative to the An-rich peak (M2), with a ratio of 0.1–4.6 (M1:M2; average 1.8). For those crystals that show only one component, this is typically at $An_{56–67}$. Of the mafic inclusion plagioclase, only 7 % of crystals have X_{An} distributions with two components: one at $\sim An_{60}$ and one at $\sim An_{76}$. This time, the An-rich peak (M2) is dominant in area relative to M1, with a ratio of ~ 0.7. The majority of mafic inclusion plagioclase crystals are fitted best by a single Gaussian with peak value at $An_{60–83}$, representing the main bulk of plagioclase crystallisation from the mafic liquid.

For the andesite plagioclase with 2-peak fits, we interpret the subordinate An-rich peak to have crystallised in a more mafic melt, as outlined above. The dominant, An-poor peak is present as the crystal rim and reflects sodic overgrowth, in one of two mechanisms:

1. Due to fractional crystallisation within the mafic inclusion, as reproduced in the MELTS modelling. This would require these mafic-derived crystals to be transferred relatively late into the andesite, perhaps during ascent in the conduit, in order not to have formed an overgrowth rim during decompression crystallisation of the andesite. Alternatively, nucleation of new microlites might be more energetically favourable than overgrowth of existing grains.
2. As a result of decompression-induced groundmass crystallisation within the andesite. This would require the crystals to be transferred into the andesite early, before complete crystallisation of the mafic inclusions, to give 'seed' crystals that could be overgrown during ascent.

These two possibilities should be distinguishable by study of pumice that has ascended rapidly from the magma chamber without time for significant groundmass crystallisation. Preliminary data collected from Phase I pumices show that plagioclase microlites compositions range from An_{61} to An_{80} (average An_{73}). The presence of predominantly high-X_{An} compositions therefore suggests that (2) may be the correct interpretation, but more work is needed.

Discussion

Methodological issues

We propose that the method presented here represents a robust means of estimating the amount of disaggregated material in the groundmass of the andesite. However, there are some potential artefacts and sources of uncertainty, in addition to the errors in the fits as outlined above. Probably, the most important source of uncertainty stems from the fact that the thin sections used in the study are 2D slices through populations of 3D crystals. There are two factors that contribute to the uncertainty, and their effects act in opposing directions.

Firstly, we are counting the *number* of grains whose 2D intersections typically have distinct An-rich cores (since very few crystals are reversely zoned in the andesite). The most favourable intersection would cut through the centre of the core, while the least favourable would intersect only

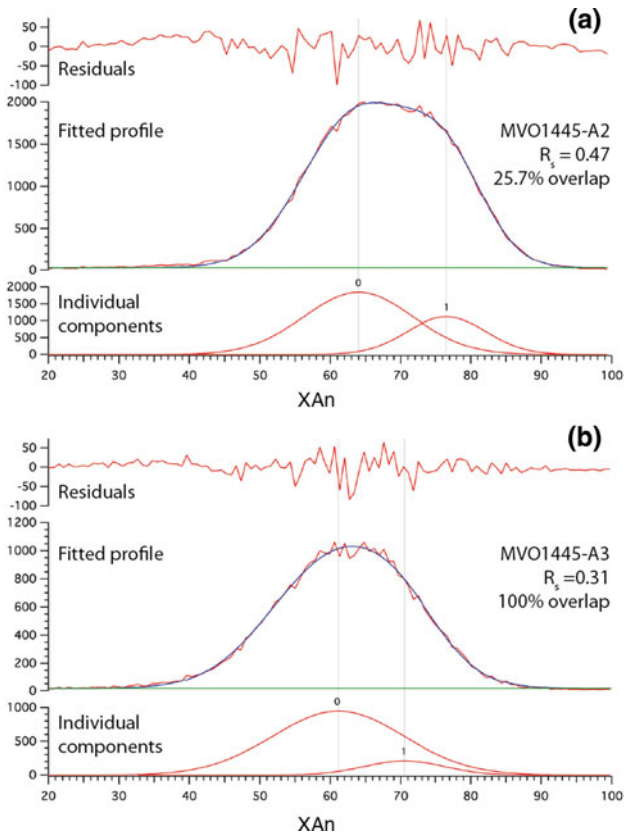

Fig. 9 Summated (bulk) X_{An} distributions for whole images, MVO1445-A2 (**a**) and MVO1445-A3 (**b**). MVO1445-A2 shows two resolvable components with peak positions at An_{64} and $An_{76.5}$. Two components cannot be successfully resolved in (**b**)

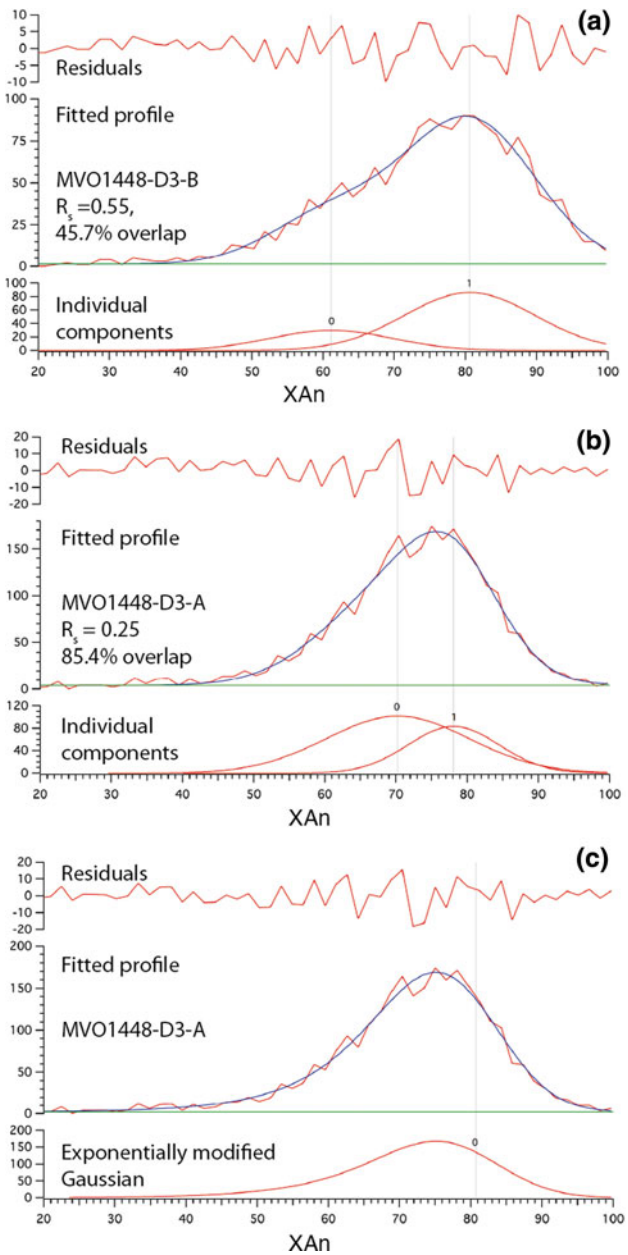

Fig. 10 Typical X_{An} distributions and fitted profiles for individual crystals from the mafic inclusion sample MVO1448. **a** Two clear components in MVO1448-D3-B, with peak locations at $An_{61.2}$ and $An_{80.6}$. $R_s = 0.55$ and the maximum overlap = 45.7 %. **b** Two components cannot be resolved in MVO1448-D3-A; the fit doesn't pass the criteria for being retained ($R_s = 0.25$ and maximum overlap = 85.4 %). **c** The same X_{An} distribution from (**b**) is matched equally well or better by an exponentially modified Gaussian curve

the outer rim of the crystal—in this instance, the crystal would not be counted even if the An-rich core is present. Clearly, the likelihood of intersecting the core depends on the relative size of the core and rim. However, in general, the use of 2D crystal populations means that we are likely to underestimate the number of crystals with An-rich cores. Converting the data set from 2D to 3D is beyond the scope of this study, and in any case, this is critically dependent on choice of the correct crystal shape or aspect ratio (Higgins 1994; Jerram and Higgins 2007). This probably varies with degree of undercooling and hence crystal size and could therefore introduce more uncertainties than it solves.

Secondly, we are measuring the relative area contribution of the An-rich core in those cases where it is identified. The relative 2D area occupied by the core is high relative to its 3D volumetric importance. For example, a crystal with a 10 × 20 × 50 μm core and a 2-μm-thick outer rim has a core volume of 1×10^4 μm^3 and a rim volume of 8,144 μm^3: the core represents 55 % of the total volume of the crystal. In contrast, the same crystal sectioned parallel to its axes has a core area of 200–1,000 μm^2 and rim of 136–296 μm^2, depending on the exact orientation of the section: the core represents 59–77 % of the total area of the crystal. Thus, a 2D section that cuts through the centre of a crystal is likely to overestimate the volumetric significance of an An-rich core. This effect is probably less significant than the effect of slices that do not intersect the crystal centre or do not intersect the core at all. This implies that we are producing minimum estimates of the significance of the mafic component in the crystals. There is no easy

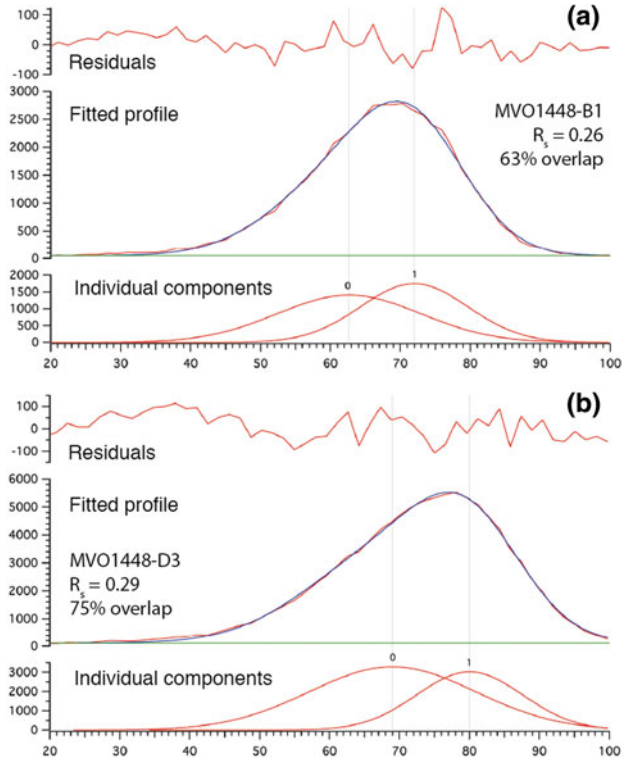

Fig. 11 Summated (bulk) X_{An} distributions for whole images, MVO1448-B1 (**a**) and MVO1448-D3 (**b**). Two components cannot be successfully resolved in either case, with $R_s < 0.31$ and overlaps >61 %

answer to these two issues, but the large number of individual crystals measured in this study should significantly help to mitigate the effects of both the under-estimate of the number of An-rich cores and the over-estimate of the core volumes.

Additional uncertainties include the presence of cracks and mineral inclusions (which typically represent relatively small total area and in some cases can be excluded from the area analysed), the accuracy of calibrations, and issues around crystals with common boundaries (e.g. where two crystals have grown into one another). In general, the greyscale calibrations presented here are good (typically with $R^2 > 0.90$) but this relies on high-quality images as well as reliable electron-probe analyses. Image quality in turn depends strongly on sample preparation (in particular on the quality of the polish) as well as resolution and signal to noise ratio. We would recommend stacking multiple images in order to improve the latter (as suggested by Ginibre et al. 2002).

The total contribution of mafic magma to the SH volcanic system

We have demonstrated that there is a greater amount of mafic magma in the volcanic system at Montserrat than can be seen in the total number of macroscopic mafic inclusions. In order to estimate the true total contribution of mafic magma, we need to account for the following components, assuming 40 % phenocrysts and 60 % matrix from point counting:

- Macroscopic mafic inclusions: these represent approx 5–8 % by area on 2D surfaces in Phases III and V (Barclay et al. 2010; Plail et al. 2012).

$$\text{Total contribution}: 5-8\,\% \text{ of the magma} \quad (2)$$

- Disequilibrium growth or reactive overgrowth on phenocrysts occurs while they are incorporated in the mafic inclusions. This affects ~25 % of all plagioclase, amphibole and orthopyroxene phenocrysts in the andesite (see Table 1). We make the conservative estimate that the amount of these crystals that crystallised in the presence of mafic melt is on average ~20 % of the crystal. This takes into account the fact that some of the disequilibrium growth may include partially reacted phenocryst material (e.g. for sieved plagioclase).

$$\text{Total contribution}: 40\,\% \text{ phenocrysts} \times 0.25 \times 0.20 = 2\,\% \text{ of the magma} \quad (3)$$

- Crystal clusters formed by disaggregating mafic inclusions: 0–2.4 % by area of the sample over nine samples, quantified by point counting as described earlier and summarised in Table 1. Normalising for sample vesicularity (approximately 16–59 %), this equates to 0.1–3.0 % by area of the sample.

$$\text{Total contribution}: 0.1-3\,\% \text{ of the magma} \quad (4)$$

- Microlites derived from disaggregation of mafic inclusions: 15.8 % of all plagioclase microlites on average (of which an average of ~45 % is represented by the An-rich cores), as quantified using the new X_{An} distribution method. We assume that the modal abundance of plagioclase in the phenocrysts (~70 % plagioclase) is also representative of the microlites and that the typical andesite retains ~30 % matrix glass (i.e. the initial 60 % matrix has crystallised by 50 % to form a groundmass).

$$\text{Total contribution}: 60\,\% \text{ matrix} \times 50\,\% \text{ groundmass crystallisation} \times 70\,\% \text{ plagioclase in the groundmass} \times 15.8\,\% \text{ of plagioclase microlites} \times \text{cores representing } 45\,\% \text{ of those microlites} = 1.5\,\% \text{ of the magma} \quad (5)$$

If we assume that groundmass clinopyroxene, orthopyroxene and oxide are affected in a similar way, this value becomes ~2.1 %.

Table 4 Results of 2-component fits to mafic inclusion plagioclase

Image	Crystal	M1	SD1	A1	W1	M2	SD2	A2	W2	Area ratio	Max overlap (%)	Total area (pixels)	Resolution (Rs)	M2-M1
MVO1448-A1	AD	64.7	6.13	1,763	14.4	76.7	5.36	2,676	12.6	0.7	31.4	4,440	0.52	12.0
MVO1448-A3	W	65.3	7.05	698	16.6	78.2	5.54	1,886	13.1	0.4	43.0	2,584	0.51	12.9
	AC	49.4	5.54	227	13.0	67.6	8.13	1,050	19.2	0.2	42.2	1,276	0.67	18.2
MVO1448-B1	X	57.7	7.52	689	17.7	70.3	7.07	1,058	16.6	0.7	46.8	1,746	0.43	12.6
	AH	65.3	4.05	310	9.5	77.2	5.74	768	13.5	0.4	37.3	1,078	0.61	11.8
	AI	57.9	8.66	1,709	20.4	71.8	6.81	3,921	16.0	0.4	48.6	5,630	0.45	14.0
MVO1448-D3	B	61.2	8.57	641	20.2	80.6	9.17	1,975	21.6	0.3	45.7	2,615	0.55	19.4
	E	65.0	8.79	980	20.7	81.7	8.09	2,160	19.1	0.5	44.7	3,140	0.50	16.7
	S	57.3	9.98	551	23.5	75.2	7.14	721	16.8	0.8	31.7	1,272	0.53	18.0
	AM	53.7	5.39	612	12.7	66.1	6.72	2,132	15.8	0.3	56.2	2,744	0.52	12.5
	AN	60.5	9.74	1,603	22.9	76.5	7.29	1,616	17.2	1.0	34.2	3,220	0.47	16.0
MVO1448-D4	J	49.7	4.18	92	9.8	64.5	5.45	352	12.8	0.3	25.2	444	0.77	14.8
	Z	59.2	4.39	121	10.3	72.4	4.77	427	11.2	0.3	27.2	548	0.72	13.2
MVO1448-D5	L	72.7	5.74	294	13.5	85.7	5.59	264	13.2	1.1	26.4	558	0.58	13.0
	AE	63.5	6.53	273	15.4	80.1	5.68	199	13.4	1.4	20.4	472	0.68	16.6
	AJ	59.9	8.28	909	19.5	79.0	8.99	2,502	21.2	0.4	43.4	3,411	0.55	19.0
	AM	68.3	7.61	467	17.9	83.4	5.87	162	13.8	2.9	45.3	629	0.56	15.1
	AO	63.4	9.09	1,890	21.4	82.0	8.20	1,575	19.3	1.2	30.9	3,465	0.54	18.7
	AT	53.5	8.80	140	20.7	75.1	9.41	379	22.2	0.4	37.4	519	0.60	21.6
	BD	55.8	9.68	623	22.8	79.3	9.16	1,033	21.6	0.6	26.9	1,656	0.62	23.4
Average		60.2				76.2				0.70				
SD		6.0				5.8				0.6				

M X_{An} location of peak, *SD* standard deviation of peak, *A* area under peak, *W* full width at half maximum, Area ratio = A1/A2

Thus, the total 'cryptic' contribution of mafic magma in the Soufrière Hills magmatic system is probably ~6 %, *in addition to* the macroscopic mafic inclusions, which are reported as ~5–8 % in Phase III (see earlier). In addition to this, there must be a melt component as the inclusions were not 100 % crystallised after magma mixing. A melt component may be difficult to recognise, particularly if there is time for extensive diffusive homogenisation, but high-K_2O glass compositions have been suggested as a signature of incompletely mixed, mafic-derived melt at Soufrière Hills Volcano (Humphreys et al. 2010). Thus, the total amount of mafic magma is far greater than would normally be recognised by simply recording the proportion of macroscopic mafic inclusions. This in itself may be a conservative estimate, because we have only included the contribution of the high-X_{An} plagioclase *cores* in the calculation above. This approach assumes that the low-X_{An} overgrowths formed in the andesite during decompression-driven crystallisation (scenario 2 as outlined earlier) and that disaggregation occurs during mingling in the magma chamber. The alternative (scenario 1) is that disaggregation occurs after mingling and in periods of high shear during magma ascent from the chamber. If this were the case, the whole crystal including the rim should be accounted for, since many of the mafic-derived plagioclase are already normally zoned, and there would be less opportunity for decompression-driven overgrowth.

Groundmass heterogeneity

Individual images from a single sample of the andesite, showing regions of groundmass approximately of 0.6 × 0.6 mm, have wide variations of the total number of microlites identified as having a mafic origin (from ~3 to >30 %, Table 2). We consider that this heterogeneity may be significant. The groundmass texture is commonly heterogeneous on the scale of a few tenths of a millimetre. This heterogeneity is most obviously identified as a variable vesicularity or 'density' in BSE images; however, the optically 'high-density' groundmass tends also to have a higher abundance of pyroxenes and oxides than the 'low-density' groundmass (Fig. 13). We suggest that the origin of this heterogeneity may be either (1) the disaggregating remnants of mafic inclusions or possibly (2) the products of hybridisation: in situ crystallisation of mafic magma that is more thoroughly mixed into the andesite than could be

Table 5 Results of MELTS modelling of fractional crystallisation of mafic inclusion composition at 200 MPa, QFM + 2

Run	Initial H_2O	Initial CO_2	Liquidus T °C	X_{An} at liquidus	X_{An} at 850 °C	% melt at 850 °C	Exsolved H_2O?	SiO_2 of residual liquid at 850 °C	Crystallising assemblage
A	0	0	1,272.3	72.2	1.5	4.5	No	79.2	fsp, opx, cpx, mt, ilm, qz
B	0.5	0	1,236.9	84.0	26.2	14.8	No	74.3	fsp, opx, cpx, mt, ilm
C	1	0	1,204.9	85.5	35.9	20.1	No	70.5	fsp, cpx, opx, mt
D	1.0	0.5	1,201.4	85.5	34.6	20.1	No	69.0	fsp, cpx, opx, mt
E	1.0	1.0	1,197.5	85.4	33.2	20.3	No	67.5	fsp, cpx, (ol), opx, mt
F	2.0	0	1,149.8	87.9	40.5	26.0	Yes	67.1	fsp, cpx, mt, opx
G	2.0	0.5	1,147.1	87.8	46.7	28.0	Yes	64.8	fsp, cpx, mt, opx
H	4.0	0	1,096.1	89.9*	37.8	30.0	Yes	64.2	cpx, mt, fsp, opx

* When plagioclase starts to crystallise at 1,062 °C

Starting composition: 49.07 wt% SiO_2, 0.90 TiO_2, 20.18 Al_2O_3, 8.95 wt% Fe_2O_3(T), 0.17 wt% MnO, 5.46 wt% MgO, 10.50 wt% CaO, 2.52 wt% Na_2O, 0.42 wt% K_2O

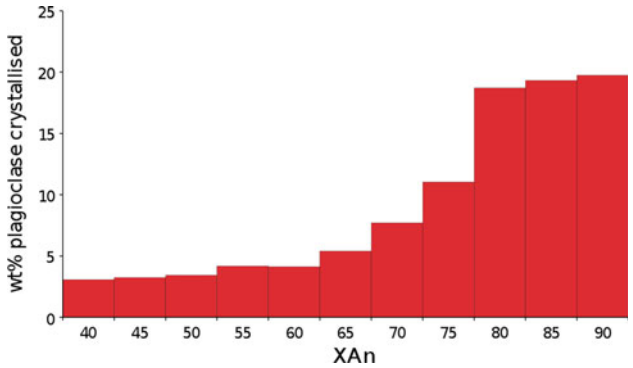

Fig. 12 X_{An} distribution produced by MELTS modelling of fractional crystallisation of a mafic inclusion bulk composition with 2 wt% H_2O. The starting composition is that of the most mafic inclusion from Barclay et al. (2010). The shape of the distribution corresponds well with the *left-hand* skewed distributions extracted from plagioclase in the mafic inclusion (see text for discussion)

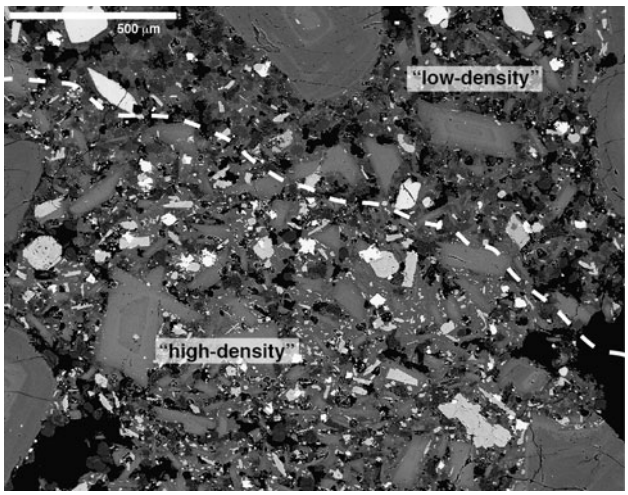

Fig. 13 Back-scattered electron image illustrating the typical heterogeneity observed in the groundmass of the andesite. The heterogeneity is clearest as 'high-density' and 'low-density' patches of groundmass; the high-density patches appear richer in pyroxenes and oxide crystals

achieved by forming a mafic inclusion. In either case, more detailed textural study of mixed magmas would be worthwhile.

Steady state and the lack of systematic bulk rock chemical signature

The identification of a substantial component of mafic magma cryptically dispersed into the andesite raises an important question regarding the long-term evolution of the magmatic system. For fifteen years in the current eruption (and over the last c. 170 ka, Harford et al. 2002), mafic magma is thought to have been intruding the volcanic system, reheating and mixing with the andesite, and causing it to erupt at the surface. At least in the current eruption products, samples show evidence of recent reheating (e.g. Ti–rich oxide phenocryst rims and microlites, Devine et al. 1998); inferred timescales are typically short (a few weeks; Devine et al. 2003). If we assume that most samples of the andesite include the ~6 vol% mafic material identified in this study, then the current eruption of ~1 km^3 (Wadge et al. 2010) has involved cryptic input of 60 million m^3 of mafic magma in addition to the 10–120 million m^3 of mafic inclusions, that is, a total of ~0.07–0.18 km^3. Yet there is no clearly observable, systematic change of the bulk andesite geochemistry towards more mafic compositions, to indicate progressive contamination of resident andesite with mafic components. A long-term change to the temperature of the resident magma might also be anticipated (Devine et al. 2003; Devine et al. in press). One possible explanation for this lack of systematic geochemical signature may lie in the almost co-linear geochemical systematics of mafic inclusion and andesite compositions (e.g. Zellmer et al. 2003), such that the bulk mafic inclusion composition is very similar to the andesite; a small amount

of two-component mixing may not yet be observable. However, the andesite storage region would need to be large, and well mixed, in order for such a long-term signature not to be identified. Alternatively, could the mafic contribution to the magmatic system have varied over time, and if so, how would this affect the eruptive behaviour? This could be tested by quantifying the cryptic mafic component in the andesite, using the methods outlined here, in samples from the full 15 years of the eruption. We suggest that careful monitoring of geochemical variables that are likely to pick up long-term trends (e.g. La/Yb, based on analyses by Zellmer et al. 2003, or isotope systematics) would be valuable.

Alternative explanations for the lack of a systematic change to bulk rock compositions include that only small amounts of andesite are being remobilised and erupted at any given time. This would require frequent input of mafic magma into the shallow crust in order to remobilise these small batches of andesitic magma, but the short reheating timescales and lack of systematic bulk rock signature could be explained by this mechanism (Devine et al. 2003).

Finally, it is also possible that the hybridised, cryptic component could be derived from slow disaggregation of old inclusions that are unrelated to the present eruption, in which case one might only expect to see temporal variations over very long timescales (e.g. of order 10 ka). We can place some constraints on the amount of time elapsed since disaggregation of the mafic inclusions, because of the observation that although scattered, plagioclase microlite cores have high MgO relative to rims. Mg diffuses relatively quickly through the plagioclase structure, with diffusivity values of 2.25×10^{-5} to 5.16×10^{-7} $\mu m^2/s$ at 850 °C, for An_{40} to An_{80}, respectively, (Costa et al. 2003). The characteristic diffusion lengthscale (the distance at which the concentration reaches the midpoint between maximum and minimum at a given time) is $x_c = \sqrt{(4Dt)}$, where D is the diffusivity and t is the time. For 850 °C and lengthscales appropriate for typical microlites, $\sim$100 μm, the diffusion time is of the order 7–307 years for An_{40} to An_{80}. This suggests that most of the disaggregated cryptic component from the mafic magma is transferred into the andesite within the last one or two eruptive episodes.

Mingling, hybridisation and mass transfer

A surprising result of this study is that nearly a quarter of all the phenocrysts in the andesite have spent long enough within the mafic magma for disequilibrium to manifest itself by the formation of reaction rims, sieve textures or new growth. These crystals are transferred from the andesite into the mafic magma during mingling, while the two magmas are still fluid (e.g. Clynne 1999; Browne et al. 2006). The textures of the mafic inclusions imply that they crystallise rapidly and comprise rigid frameworks of interlocking small crystals, but the inclusions are also highly vesicular and may still be permeable to gas flow and melt percolation. The inherited phenocrysts can be transferred back into the andesite either while the mafic magma is still liquid (giving a very short time window for incorporation, reaction, overgrowth and transfer back to the andesite) or while it is solid. We suggest that the latter is more likely and that this could occur either by disaggregation of still plastic inclusions as a result of shearing due to magma flow or possibly by bursting of mafic inclusions ('auto-fragmentation') due to volatile overpressure resulting from second boiling. This raises the question of why pargasitic amphibole microlites are not observed in the groundmass of the andesite, as at Unzen (Sato et al. 1999), when approximately one-third of the mafic inclusions contain appreciable amphibole (Plail et al. 2012); this was commented on by both Murphy et al. (2000) and Couch et al. (2003). We suggest that differences in the initial volatile content, and/or the strength of the mush framework between amphibole-bearing and px-plag mafic inclusions might explain this apparent difference in preservation. The amphibole-bearing inclusions may represent different initial melts (Plail et al. 2012) and tend to have strongly chilled margins, which would increase the strength of the inclusions and decrease the likelihood of disaggregation.

Conclusions

1. Approximately 25 % of all phenocrysts in the Soufrière Hills andesite have undergone significant interaction with mafic magma. This points to very significant mass transfer between the resident and recharging magmas.
2. X_{An} distributions retrieved from back-scattered electron images of plagioclase can be used to identify and quantify groundmass crystals that originated in mafic inclusions
3. The total amount of cryptic, disaggregated mafic material in the andesite is significant, at least 6 % by area in a sample of andesite from Phase III.
4. This method could be used in future to determine whether the amount of mafic material has changed with time and as a consequence will allow assessment of the significance of mafic magma supply for the volatile budget and for monitoring data sets.
5. The presence of cryptic mafic-derived material may be linked to strong sub-mm scale heterogeneity in the andesite groundmass; detailed textural studies of the andesite groundmass would be worthwhile.

Acknowledgments We acknowledge useful discussions with Kathy Cashman, Dan Morgan, Steve Sparks, Geoff Wadge, Paul Cole, Richard Katz and Vicki Smith, who also provided analytical support. MCSH was supported by a Royal Society University Research Fellowship. ME acknowledges support from COMET+, the NERC National Centre for Earth Observation. MP was supported by a NERC studentship. We acknowledge funding from NERC grant NE/I008543/1. Useful reviews were received from Mike Clynne and Pavel Plechov, which, together with suggestions from editor Jon Blundy, helped improve the manuscript.

References

Bacon CR (1986) Magmatic inclusions in silicic and intermediate volcanic rocks. J Geophys Res 91:6091–6112

Barclay J, Herd RA, Edwards BR, Christopher T, Kiddle EJ, Plail M, Donovan A (2010) Caught in the act: implications for the increasing abundance of mafic enclaves during the recent eruptive episodes of the Soufriere Hills Volcano, Montserrat. Geophys Res Lett 37:L00E09

Baxter PJ, Bonadonna C, Dupree R, Hards VL, Kohn SC, Murphy MD, Nichols A, Nicholson RA, Norton G, Searl A, Sparks RSJ, Vickers BP (1999) Cristobalite in volcanic ash of the Soufrière Hills Volcano, Montserrat, British West Indies. Science 283:1142–1145

Blundy JD, Sparks RSJ (1992) Petrogenesis of mafic inclusions in granitoids of the Adamello Massif, Italy. J Petrol 35:1039–1104

Browne BL, Eichelberger JC, Patino LC, Vogel TA, Dehn J, Uto K, Hoshizumi H (2006) Generation of porphyritic and equigranular mafic enclaves during magma recharge events at Unzen Volcano, Japan. J Petrol 47:301–328

Cashman KV (1992) Groundmass crystallisation of Mount St. Helens dacite, 1980–1986: a tool for interpreting shallow magmatic processes. Contrib Mineral Petrol 109:431–449

Clynne MA (1999) A complex magma mixing origin for rocks erupted in 1915, Lassen Peak, California. J Petrol 40:105–132

Coombs ML, Eichelberger JC, Rutherford MJ (2002) Experimental and textural constraints on mafic enclave formation in volcanic rocks. J Volcanol Geotherm Res 119:125–144

Costa A (2005) Viscosity of high crystal content melts: dependence on solid fraction. Geophys Res Letters 32:L22308

Costa F, Chakraborty S, Dohmen R (2003) Diffusion coupling between trace and major elements and a model for calculation of magma residence times using plagioclase. Geochim Cosmochim Acta 67:2189–2200

Couch S, Harford CL, Sparks RSJ, Carroll MR (2003) Experimental constraints on the conditions of formation of highly calcic plagioclase microlites at the Soufrière Hills Volcano, Montserrat. J Petrol 44:1455–1475

D'Lemos RS (1996) Mixing between granitic and dioritic crystal mushes, Guernsey, Channel Islands, UK. Lithos 38:233–257

Devine JD, Murphy MD, Rutherford MJ, Barclay J, Sparks RSJ, Carroll MR, Young SR, Gardner JE (1998) Petrologic evidence for pre-eruptive pressure-temperature conditions, and recent reheating, of andesite magma erupting at the Soufrière Hills Volcano, Montserrat, WI. Geophys Res Lett 25:3669–3672

Devine JD, Rutherford MJ, Norton GE, Young SR (2003) Magma storage region processes inferred from geochemistry of Fe-Ti oxides in andesitic magma, Soufrière Hills Volcano, Montserrat, WI. J Petrol 44:1375–1400

Druitt TH, Costa F, Deloule E, Dungan M, Scaillet B (2012) Decadal to monthly timescales of magma transfer and reservoir growth at a caldera volcano. Nature 482:77–80

Edmonds M, Aiuppa A, Humphreys M, Moretti R, Giudice G, Martin RS, Herd RA, Christopher T (2010) Excess volatiles supplied by mingling of mafic magma at an andesite arc volcano. Geochem Geophys Geosys 11:Q04005

Eichelberger JC (1978) Andesitic volcanism and crustal evolution. Nature 275:21–24

Eichelberger JC, Chertkoff DG, Dreher ST, Nye CJ (2000) Magmas in collision: rethinking chemical zonation in silicic magmas. Geology 28:603–606

Elsworth D, Mattioli G, Taron J, Voight B, Herd R (2008) Implications of magma transfer between multiple reservoirs on eruption cycling. Science 322:246–248

Feeley TC, Dungan MA (1996) Compositional and dynamic controls on mafic-silicic magma interactions at continental arc volcanoes: evidence from Cordón El Guadal, Tatara-San Pedro complex, Chile. J Petrol 37:1547–1577

Feeley TC, Wilson LF, Underwood SJ (2008) Distribution and compositions of magmatic inclusions in the Mount Helen dome Lassen Volcanic Center, California: insights into magma chamber processes. Lithos 106:173–189

Ghiorso MS, Sack RO (1995) Chemical mass transfer in magmatic processes. IV. A revised and internally consistent thermodynamic model for the Interpolation and Extrapolation of Liquid-Solid equilibria in magmatic systems at elevated temperatures and pressures. Contrib Miner Petrol 119:197–212

Ginibre C, Kronz A, Wörner G (2002) High-resolution quantitative imaging of plagioclase composition using accumulated back-scattered electron images: new constraints on oscillatory zoning. Contrib Mineral Petrol 142:436–448

Harford CL, Pringle MS, Sparks RSJ, Young SR (2002) The volcanic evolution of Montserrat using $^{40}Ar/^{39}Ar$ geochronology. In: Druitt TH, Kokelaar BP (eds) 2002. The eruption of Soufriere Hills Volcano, Montserrat, from 1995 to 1999. Geological Society, London, vol 21, pp 93–113

Heiken G, Eichelberger JC (1980) Eruptions at Chaos Crags, Lassen Volcanic National Park, California. J Volcanol Geotherm Res 7:443–481

Higgins MD (1994) Numerical modelling of crystal shapes in thin sections: estimation of crystal habit and true size. Am Mineral 79:113–119

Humphreys MCS, Blundy JD, Sparks RSJ (2006) Magma evolution and open-system processes at Shiveluch Volcano: insights from phenocryst zoning. J Petrol 47:2303–2334

Humphreys MCS, Christopher T, Hards V (2009a) Microlite transfer by disaggregation of mafic inclusions following magma mixing at Soufrière Hills volcano, Montserrat. Contrib Mineral Petrol 157:609–624

Humphreys MCS, Edmonds M, Christopher T, Hards V (2009b) Chlorine variations in the magma of Soufrière Hills Volcano, Montserrat: insights from Cl in hornblende and melt inclusions. Geochim Cosmochim Acta 73:5693–5708

Humphreys MCS, Edmonds M, Christopher T, Hards V (2010) Magma hybridisation and diffusive exchange recorded in heterogeneous glasses from Soufrière Hills Volcano, Montserrat. Geophys Res Lett 37:L00E06

Jerram DA, Higgins MD (2007) 3D analysis of rock textures: quantifying igneous microstructures. Elements 3:239–245

Kent AJR, Darr C, Koleszar AM, Salisbury MJ, Cooper KM (2010) Preferential eruption of andesitic magmas through recharge filtering. Nat Geosci 3:631–636

Kiddle EJ, Edwards BR, Loughlin SC, Petterson M, Sparks RSJ, Voight B (2010) Crustal structure beneath Montserrat, Lesser Antilles, constrained by xenoliths, seismic velocity structure and petrology. Geophys Res Lett 37:L00E11

Komorowski J-C, Legendre Y, Christopher T, Bernstein M, Stewart R, Joseph E, Fournier N, Chardot L, Finizola A, Wadge G, Syers

R, Williams C, Bass V (2010) Insights into processes and deposits of hazardous vulcanian explosions at Soufrière Hills Volcano during 2008 and 2009 (Montserrat, West Indies). Geophys Res Lett 37:L00E19

Kouchi A, Sunagawa I (1985) A model for mixing basaltic and dacitic magmas as deduced from experimental data. Contrib Mineral Petrol 89:17–23

Macdonald R, Hawkesworth CJ, Heath E (2000) The Lesser Antilles volcanic chain: a study in arc magmatism. Earth Sci Rev 49:1–76

Martel C, Radadi Ali A, Poussineau S, Gourgaud A, Pichavant M (2006) Basalt-inherited microlites in silicic magmas: evidence from Mount Pelée (Martinique, French West Indies). Geology 34:905–908

McLeod GW, Dempster TJ, Faithfull JW (2011) Deciphering magma-mixing processes using zoned titanite from the Ross of Mull granite, Scotland. J Petrol 52:55–82

Melnik O, Sparks RSJ (1999) Nonlinear dynamics of lava dome extrusion. Nature 402:37–41

Mortazavi M, Sparks RSJ (2004) Origin of rhyolite and rhyodacite lavas and associated mafic inclusions of Cape Akrotiri, Santorini: the role of wet basalt in generating calcalkaline silicic magmas. Contrib Mineral Petrol 146:397–413

Murphy MD, Sparks RSJ, Barclay J, Carroll MR, Lejeune A-M, Brewer TS, Macdonald R, Black S, Young SR (1998) The role of magma mixing in triggering the current eruption at the Soufrière Hills volcano, Montserrat, West Indies. Geophys Res Lett 25:3433–3436

Murphy MD, Sparks RSJ, Barclay J, Carroll MR, Brewer TS (2000) Remobilisation of andesite magma by intrusion of mafic magma at the Soufrière Hills Volcano, Montserrat, West Indies. J Petrol 41:21–42

Nakada S, Bacon CR, Gartner AE (1994) Origin of phenocrysts and compositional diversity in pre-Mazama rhyodacite lavas, Crater Lake, Oregon. J Petrol 35:127–162

Plail M, Barclay J, Humphreys MCS, Edmonds M, Herd R, Christopher T (2012) Characterisation of mafic enclaves in the erupted products of Soufrière Hills Volcano, Montserrat 1995–2010. Geol Soc Lon Memoir (accepted)

Plechov PYu, Tsai AE, Shcherbakov VD, Dirksen OV (2008) Opacitization conditions of hornblende in Bezymyannyi Volcano andesites (March 30, 1956 eruption). Petrology 16:19–35

Rasband WS, Image J (1997–2011) U. S. National Institutes of Health, Bethesda, Maryland, USA, http://imagej.nih.gov/ij/

Rutherford MJ, Devine JD (2003) Magmatic conditions and magma ascent as indicated by hornblende phase equilibria and reactions in the 1995–2002 Soufrière Hills magma. J Petrol 44:1433–1454

Ryan GA, Loughlin SC, James MR, Jones LD, Calder ES, Christopher T, Strutt MH, Wadge G (2010) Growth of the lava dome and extrusion rates at Soufrière Hills Volcano, Montserrat, West Indies: 2005–2008. Geophys Res Lett 37:L00E08

R Development Core Team (2010) R: A language and environment for statistical computing. R Foundation for Statistical Computing, Vienna, Austria. ISBN 3-900051-07-0, URL http://www.R-project.org/

Sato H, Nakada S, Fujii T, Nakamura M, Suzuki-Kamata K (1999) Groundmass pargasite in the 1991–1995 dacite of Unzen volcano: phase stability experiments and volcanological implications. J Volcanol Geotherm Res 89:197–212

Snyder et al (1997) Practical HPLC method development. Wiley, NY

Sparks RSJ, Marshall LA (1986) Thermal and mechanical constraints on mixing between mafic and silicic magmas. J Volcanol Geotherm Res 29:99–124

Sparks RSJ, Sigurdsson H, Wilson L (1977) Magma mixing: a mechanism for triggering acid explosive eruptions. Nature 267:315–318

Sparks RSJ, Murphy MD, Lejeune AM, Watts RB, Barclay J, Young SR (2000) Control on the emplacement of the andesite lava dome of the Soufrière Hills volcano, Montserrat by degassing-induced crystallisation. Terra Nova 12:14–20

Stout CM, Hammersley L, Clynne MA (2007) Field measurements of mafic enclave population density at Chaos Crags, Lassen Volcanic National Park, CA and implications for magma mixing. 103rd Annual meeting of the Geological Society of America, Cordilleran Section, abstract no. 30–12

Tepley FJ, Davidson JP, Clynne MA (1999) Magmatic interactions as reorded in plagioclase phenocrysts of Chaos Crags, Lassen Volcanic Center, California. J Petrol 40:787–806

Wadge G, Isaacs MC (1988) Mapping the volcanic hazards from Soufriere Hills Volcano, Montserrat, West Indies using an image processor. J Geol Soc Lon 145:541–551

Wadge G, Herd R, Ryan G, Calder ES, Komorowski J-C (2010) Lava production at Soufrière Hills Volcano, Montserrat: 1995–2009. Geophys Res Lett 37:L00E03

Wiebe RA (1987) Rupture and inflation of a basic magma chamber by silicic liquid. Nature 326:69–71

Zellmer GF, Hawkesworth CJ, Sparks RSJ, Thomas LE, Harford CL, Brewer TS, Loughlin SC (2003) Geochemical evolution of the Soufrière Hills volcano, Montserrat, Lesser Antilles volcanic arc. J Petrol 44:1349–1374